Distribution A: Approved for public release; distribution unlimited.

Calibration and Processing of Nortek Signature1000 Echosounders

by Christopher Bassett and Kristin Zeiden

Technical Report
APL-UW TR 2307
December 2023

Applied Physics Laboratory University of Washington
1013 NE 40th Street Seattle, Washington 98105-6698

ACKNOWLEDGMENTS

This work was performed with support from the Office of Naval Research under the UnderSea Remote Sensing (USRS) Departmental Research Initiative.

ABSTRACT

The five-beam Nortek Signature series acoustic Doppler current profilers (ADCPs) include a vertical beam that can be operated as an echosounder. These echosounders record an echo intensity level as a function of range in hundredths of a decibel. While these recorded levels provide valuable qualitative information about scattering from the water column, without calibration the units' recorded echo intensities cannot be linked quantitatively to scattering processes. In this report we summarize calibration results for six Nortek Signature1000 units. The echosounders were calibrated in the field while deployed on 4$^{\text{th}}$ generation Surface Wave Instrument Floats with Tracking (SWIFTs) by suspending 38.1-mm tungsten carbide spheres with 6% cobalt binder below. Here, we summarize the equations used to process Nortek Signature series echosounder data, general calibration procedures for echosounders, the methodology used to calibrate the six units, the results of the calibrations, and uncertainties and recommendations for future work. In addition, we present post-processed, calibrated echosounder data from a deployment of the SWIFTs equipped with the Signature1000s in Mobile Bay, Alabama.

The primary objective of this report is to support the use of the Nortek Signature1000 units on SWIFTs, a platform used widely in research performed at the Applied Physics Laboratory of the University of Washington. Recognizing that there is broader interest in the echosounder capabilities of the Nortek Signatures series, the scope of this report has been expanded beyond calibration of the available units. Ideally this report will equip users, including those less familiar with echosounders and acoustic data processing, to calibrate other Nortek Signature series instruments by similar methods. Links to processing scripts used to calibrate the units and post-process echosounder data are included.

CONTENTS

1 INTRODUCTION

The Surface Wave Instrument Float with Tracking (SWIFT) is an instrument developed at the Applied Physics Laboratory to make surface and near-surface measurements across ocean environments.[1;2] During operations, SWIFT drifters make Lagrangian measurements of upper water column velocity and turbulence. To make these measurements the 4^{th} generation SWIFT is equipped with a downward-looking Nortek Signature1000 acoustic Doppler current profiler (ADCP). The ADCP is equipped with five beams, one of which is oriented vertically. In contrast to the other beams, this fifth beam can be operated as an echosounder and records a time series of backscattering intensities in the water column. This report seeks to facilitate the broader adoption of Nortek Signature1000 echosounders by establishing procedures to convert data streams to standard, calibrated data products following well-established equations and calibration procedures.

An echosounder operates by transmitting a pulse of sound into the water and switching to receive mode to record signals scattered back to the unit. These echoes from the water column are created by fluctuations in the acoustic properties (sound speed, density) encountered by the outward propagating wave. The intensity and frequency dependence of the scattered signal is related to the material properties, size, shape, roughness, and distribution of the scatterers. Echosounders are used most commonly at frequencies ranging from 10s to 100s of kHz. Across this common range of frequencies many biological scatterers and physical scattering mechanisms have characteristic frequency dependencies (e.g., a spectral slope) that can be leveraged to discriminate among potential scattering mechanisms or help constrain forward and inverse models for quantitative interpretation.[3–8] At frequencies of 10s to 100s of kHz, circular transducers of manageable sizes can be constructed that result in highly directional beams, which are ideal for imaging the water column and performing quantitative measurements. The Nortek Signature line includes units that operate from 100 to 1000 kHz, with the Signature1000 series being the smallest unit with the highest operational frequency (nominally 1 MHz).

Regardless of manufacturer, a basic data product generated by echosounders is a measure of the intensity of echoes as a function of time, which is subsequently converted to range using sound speed. These data are used widely for quantitative purposes (e.g., fisheries acoustics[9]) and because of their high-resolution imaging capabilities. When used simply to image the water column it is not necessary to calibrate echosounders because the relative intensity of backscattering itself is often sufficient. However, calibration is necessary to derive quantitative information (i.e., data products where the intensity of acoustic backscatter is presented in units that can be related directly to scattering models) from echosounder measurements. The outcome of a calibration, here referred to as a gain, serves as a scalar factor that accounts for a number of unmeasured aspects of a system's performance that include, but are not limited to, signal generation and amplification, transducer transmit/receive sensitivities, filtering, and analog to digital conversion.

Calibrations are often performed by suspending a sphere of known properties within the beam of an echosounder to measure the on-axis beam response and beam pattern, if possible.[9–13] Because the analytical solution for scattering from a sphere (fluid or solid) is known[14;15], it is possible to account for the system's components without measuring them directly. Many factors have a role in identifying a suitable sphere, or set of spheres, for calibration. These include the material properties of the sphere, its size, and the frequencies transmitted by the echosounder.[10;12;16;17] However, once a suitable sphere is selected the basic approach to calibration is relatively straightforward, even if execution can be more difficult in practice. Through such a calibration, a term is calculated that can be used to convert raw signals measured by echosounders to the intensity of echoes using different forms of the SONAR equation. If frequency-modulated signals are used and frequency-domain analysis is of interest, the methodology is functionally similar but results in frequency-dependent calibration curves. The calibration approach adopted here adheres to the well-established methodology used for similar instrumentation.

The scope of this report is sufficiently broad that it addresses issues of general concern to Nortek Signature series echosounder users, but its focus is on facilitating the use of the Nortek Signature1000 units on the 4$^{\text{th}}$ generation SWIFT. To these ends, we provide an overview of the operations of the Nortek Signature series echosounders, describe calibration procedures centered around field measurements, and summarize post-processing scripts for calibration and standard field measurements. While focused on the Signature1000 units, the descriptions of the operations, processing, and implementation are generally applicable across different Signature series models. The code base (see Appendix) developed as part of this work produces quantitatively meaningful outputs from the Signature series echosounders in units that allow for direct comparison to those commonly encountered in the acoustics literature.

This report's sections cover topics ranging from the basic equations used to process echosounder data to examples of data processed using calibrated units. Section 2 discusses the equations applied to process the Signature series echosounder data (i.e., versions of the SONAR equation). Details regarding instrument outputs and the calculation of terms in the SONAR equations are included in Section 3. Section 4 presents background information about calibration and the specific processing applied to calibrate the Signature1000 echosounders. Results from field calibrations coupled with uncertainties and limitations to the approach are included in Section 5 ,while examples of processed data products are included in Section 8. The Appendix includes links to access the publicly available processing scripts and descriptions of the codes, which are implemented in MATLAB.

Numerous sections of this report assume a basic familiarity with echosounder systems and acoustics instrumentation and terminology. Valuable background resources are available in books such as Simmonds and MacLennan [9], and references therein.

2 GOVERNING EQUATIONS

This section presents the equations used to convert Nortek Signature series echosounder data streams into quantities of interest, including the volume backscattering strength and acoustic target strength. Throughout, we use the language and units widely adopted by the fisheries acoustics community since these are easily referenced and unambiguously described in numerous references including MacLennan et al. [18] The equations and processing herein focus exclusively on the conversion of recorded signals to volume and point scattering strength calculations in the time domain, which are used to produce echograms. An echogram is a figure that represents backscattering intensity as a function of range (y-axis) and time or position (x-axis). Users interested in frequency domain analysis of frequency modulated signals are referred to other resources. [16;17;19–21]

In volume scattering applications, the term being calculated is S_v (dB re 1/m). For single targets (e.g., an individual fish), the value of interest is the acoustic target strength [TS (dB re 1 m^2)]. The echosounder data is recorded in terms of a power level P_r. The Nortek Theory of Operations manual[22] contains the following equations to convert P_r to quantities commonly used in acoustic scattering applications:

$$S_v = P_r + 20\log_{10} R + 2\alpha R + PL - 10\log_{10}\left(\frac{c\tau}{2}\right) - \Psi + G_{int} \tag{1a}$$

$$TS = P_r + 40\log_{10} R + 2\alpha R + PL + G + B(\theta), \tag{1b}$$

where S_v is the logarithmic form of the volume backscattering cross section (σ_v), R is the range, $2\alpha R$ accounts for attenuation in both directions, PL represents a power level in dB referenced to 0 at maximum power, $10\log_{10}\left(\frac{c\tau}{2}\right)$ accounts for the length of the pulse where τ is the pulse duration, Ψ is the equivalent beam angle (dB re 1 steradian), and G_{int} is a gain calculated for scattering from a target integrated over a volume that includes the effects of a finite pulse duration. Note that Equation 1a lacks a term for the echosounder source level, which is accounted for by the gain term.

Equation 1b describes the logarithmic form of the backscattering cross-section (σ_{bs}) regularly applied for single targets within the beam. Thus, the only terms in the equation are the received power levels, compensated for spherical spreading in both directions, a term to account for attenuation, the instrument's relative power level, the calibration gain (G), and a term (B) to account for the changes in the intensity of the beam for off-axis targets. Here, the notation "G" is used to differentiate the gain from G_{int} given that the latter term is derived from integration of the scattered signal while the former is not. Given that the Nortek Signature series units lack capabilities to localize a target within the beam, the B term is not further discussed here.

Missing from both Equations 1a and 1b, but included in Nortek's documentation, is the subtraction of a noise term. Recommendations for implementing this in future work are discussed in Section 7.

The different terms in the S_v and TS equations account for assumptions inherent in volume and point scattering measurements. For example, calculation of S_v requires accounting for the ensonified volume as a function of range. In contrast, the calculation of acoustic target strength assumes a relatively small, single target ensonified by the beam. In both cases, the transmitted sound spreads spherically and is attenuated leading to a decrease in the signal's power as a function of range. Thus, both applications include time-varying gain terms required to account for signal intensity as a function of range.

The use of these terms is well established in the literature and can be reviewed in references including, but not limited to Medwin and Clay [23], MacLennan et al. [18], and Simmonds and MacLennan [9]. TS and S_v are related such that if a beam contains distributed targets of the same backscattering cross section that satisfy linearity requirements [24] then

$$\sigma_v = \rho_v \sigma_{bs} \tag{2a}$$

$$S_v = 10\log_{10}(\rho_v) + TS, \tag{2b}$$

where ρ_V is the volumetric density of targets [number/m^3] in the beam.

Note that Equation 1a, which is included in the Theory of Operation document provided by Nortek [22], is valid for narrowband measurements with range resolution determined by the pulse duration. The Signature series echosounders can transmit both narrowband or frequency-modulated signals and can be programmed to provide different output resolutions. Equation 1a is therefore not generally applicable and is inconsistent with other definitions provided elsewhere in the literature when applied to pulse-compressed, frequency-modulated signals. For pulse-compressed broadband signals or any signals averaged to obtain a resolution greater than the inherent resolution, this term can be replaced with a more generalized form relating to the range resolution of the measurements (ΔR) according to $10\log_{10}(\Delta R)$. In addition, note that the combined Ψ, ΔR, and an additional R^2 term that is absorbed into the spreading term to give the $20\log_{10} R$ in Equation 1a term collectively account for the volume of the beam at a given range.

Most of the terms in Equations 1b and 1a are derived directly from the underlying physics and systems settings. However, due to electrical and mechanical system design and dependencies on environmental conditions, it is best to calculate terms Ψ, G_{int}, and G through calibration. In practice, Ψ can be difficult to measure with echosounders that are not constructed from multiple sectors to allow for array processing unless a facility capable of making precise measurements is available. Here, approximations based on the analytical solution for piston transducers are applied (see Sec. 3 for details). The gain terms, G and G_{int} are most often determined using sphere calibration techniques, which are described in detail in Section 4.

Note again that this report is focused primarily on the use of Signature1000 units in the context of measurements using the SWIFT drifters. Their general operations and telemetry requirements motivate the use of range-binned scattering measurements rather than raw signals to limit data volumes. The data streams, as described below, are processed with relatively low resolution compared to operational alternatives including pulse-compressed, raw signals. For frequency-modulated, pulse-compressed signals, including those using Signature series echosounder data, alternative formulations and associated discussions can be found in numerous manuscripts and reports. [13;17;19;20;25]

Revisiting Equation 1a, we insert ΔR in place of the $\frac{c\tau}{2}$ term to calculate S_v for the system outputs. The formulation implemented in processing of field measurements and calibration data is then:

$$S_v = P_r + 20\log_{10} R + 2\alpha R + PL - 10\log_{10} \Delta R - \Psi + G_{int} \tag{3}$$

Because a vector for R is calculated from the time delay associated with an echo, α is associated with water properties, and PL and ΔR are dictated by system settings; if Ψ is known (Section 3) then G_{int} can be determined by Equation 3.

For a good calibration the objective is to have the sphere be the sole, significant contributor to measured backscattering at a given range. To solve for the calibration gain, we first leverage the relationships described in Equations 2a and 2b and introduce a new term, the area backscattering coefficient (s_a). In general, the gain is solved by relating the theoretical area backscattering coefficient ($s_{a,th}$) to the measured value ($s_{a,m}$) compensated for the arithmetic form of the gain (g_{int}) such that

$$s_{a,th} = s_{a,m} + g_{int}. \tag{4}$$

Note that TS has units of dB re 1 m^2 while S_v has units of dB re 1/m. These units can be made to match by calculating the area backscattering coefficient (s_a) from S_v such that

$$s_{a,m} = \int_{R_{min}}^{R_{max}} 10^{S_{v,uncal}/10} dz, \tag{5}$$

where $S_{v,m}$ is the S_v (Equation 3) calculated with all terms except the gain (G_{int}), which remains unknown. This results in a unitless value. Similarly, the theoretical TS of the sphere is converted to a unitless value according to

$$s_{a,th} = \frac{10^{TS_{th,ave}/10}}{10^{\Psi/10} R_s^2}, \tag{6}$$

where the denominator is the area ensonified by the beam at the range of the sphere (R_s) and the numerator is the average theoretical target strength across the transmitted band. Setting these values equal, rearranging the equations to solve for the calibration constant, and changing the integral in Equation 6 to its discrete form yields

$$G_{int} = 10\log_{10}\left(\frac{10^{TS_{th,ave}/10}}{10^{\Psi/10}\ R_s^2}\right) - 10\log_{10}\left(\left(\sum_{i=min\ R}^{i=max\ R} 10^{(S_{v,uncal}(R_i))/10}\right)\Delta R\right), \tag{7}$$

where ΔR is the total thickness of the layer around the sphere selected for analysis, R_s corresponds to the range to the sphere, and i is an index associated with the range bins. Equation 7 is simply a rearranged form of Equation 4, which accounts for the integrated but uncalibrated S_v values and the theoretical target strength and beamwidth to produce the final gain value in units of dB and can be derived from echo integrator formulations.[9;26]

Using the equations highlighted in this section one can calculate standard quantitative products from the Signature series echosounder data streams. Sections 3–4 describes how these data streams are used to solve these equations for the calibration gains and implement them for general processing. Equations 3–7 focus on calibration for volume backscattering. In point scattering applications, the gain is calculated by rearranging Equation 1b. Details of this approach are presented in Section 4.

3 CALCULATIONS USING THE SIGNATURE1000 DATA STREAMS

Several options are available for programming the Signature units. The transmit signal power level, pulse type and duration, and range resolution are of particular relevance in the application of the SONAR equations (Equations 1a and 1b). The SWIFT-mounted echosounders are configured to use a frequency-modulated transmit signal that is 0.1-ms in duration. The center frequency of the frequency-modulated signal is 1 MHz and the total bandwidth is 25%, or 250 kHz centered around the unit's nominal frequency. Thus, the transmit signal used here sweeps from 875-1125 kHz. Power level for the Nortek Signature units is defined relative to the maximum intensity transmit signals and has options ranging from –12 dB to 0 dB. This term appears as a scalar offset on the SONAR equations. Here we have used PL = –10 dB. While we would expect that the system's power level would scale as intended with the programming of the PL, we have not performed measurements to verify it.

Once the signal is transmitted the units switch to receive the signals. The echosounder requires a small, but finite amount of time to switch from transmit to receive mode and to allow for vibrations of the transducer to dissipate. The time between the end of the transmit signal and the beginning of the measurements of the received signal is referred to as the blanking distance. By default, the Nortek Signature echosounders apply a nominal sound speed of 1500 m/s to convert from time to range. A vector of ranges for each ping is determined from the combination of the programmed blanking distance (r_{blank}) and cell size (or bin range size, dr_{sig}) according to $r_{sig} = r_{blank} + [0 : N-1] * dr_{sig} + dr_{sig}/2$, where N is the total number of range bins recorded and the range is calculated in the middle of each bin. Given that the Nortek Signature units record data as a function of range assuming this nominal value, a scalar modification to recorded range bins is ultimately required to account for the measured or estimated sound speed.

The codes used here and provided for future processing necessarily account for environmental variability. For any individual burst of pings, this value can be modified through user inputs of water properties. The Signature echosounder's range vector is remapped according to $r = r_{sig} * (c/c_{sig})$, where the subscript $_{sig}$ again refers to the default values and c is the sound speed determined by the user inputs according to Fofonoff and Millard (1983).[27] If no water properties are input, the code reverts to default values of 30 PSU, 10°C, a mean water depth of 10 m, and a pH of 8.1. These values yield a sound speed of 1493.9 m/s. These corrected range values are used to calculate the time-varying gain terms including the compensation for spreading and attenuation. This correction, when applied to the spreading terms, is small (i.e., < 1 dB) over the operational range of the Signature1000.

Regardless of their pulse configuration (e.g., continuous wave versus frequency modulated) the received signals recorded by the echosounders, denoted by P_r, are provided in units of 100^{th}s of a dB. The processing codes associated with this report immediately convert this value to decibels by $P_r = 0.01 P_{r,sig}$ [dB], where the *sig* subscript again denotes the value recorded by the echosounder. Once converted to decibels, P_r is integrated directly into TS and S_v with no further modifications. Note that this approach varies from that applied by some other echosounders (e.g., the Simrad EK60[12] and EK80[17;20]), that use modified versions of the SONAR equations built around a power budget. These differences are ultimately accounted for by the calibration gains.

The echosounders on the SWIFTs are programmed to provide data using 4-cm range bins based on the unit's nominal sound speed. Prior to recording P_r for each of these bins the received signals are pulse compressed (matched filtered)[19;28] using the idealized replica of the transmitted signal. The arithmetic mean of the pulse compressed signal over each 4-cm window is then converted to dB and stored for each ping. This is all performed on the unit and not in post-processing. Note that the range resolution of an ideal, frequency-modulated chirp is approximately $dR = c/2BW$, where BW is the transmitted bandwidth.[19;25;28] This value is significantly less than the averaging window. As a result, the peak of a pulse-compressed signal corresponding to a single target is averaged out across the lower resolution window. While not generally problematic, this must be accounted for if attempting to calibrate the gain for point scattering operations (Section 5).

The range dependent (spreading) terms in the SONAR equation require no modification to the range vector beyond accounting for the local sound speed. To account for the attenuation of the signal the supporting codes use the formulations of Francois and Garrison[29;30] If no water properties are passed to the scripts then the defaults are the same as those used to modify the range vector. The scripts attached also assume that the transmit pulse is a frequency modulated chirp (875–1125 kHz). To determine α the attenuation is calculated for the full frequency range with 1-kHz resolution and the final attenuation value is determined by the arithmetic mean of values across the range converted back to units of dB/m. That is, $\alpha = 10log_{10}(\overline{\alpha(f)})$. For the Lake Washington calibrations described here $\alpha = 0.34$ dB/m. Note that the operational frequency of the Signature1000 is sufficiently high that the viscous effects in fresh water dominate the contributions to attenuation.

The equivalent beam angle represents the combined transmit and received beam patterns and is defined by

$$\psi = \int_0^{2\pi} \int_0^{2\pi} b_R(\theta, \phi) b_T(\theta, \phi) \sin(\theta) d\theta d\phi, \tag{8}$$

where b_R and b_T are the receive and transmit beam patterns, respectively, and its logarithmic form is $\Psi = 10\log_{10}(\psi)$. The equivalent beam angle can be measured using a series of precise measurements that place a target at a known range and location in the beam. For piston-like transducers with no shading of the elements an approximation of this equation, valid for large values of ka, converted to logarithmic form, is given by

$$\Psi(k) = 10\log_{10}\left(\frac{5.78}{(ka)^2}\right), \tag{9}$$

where k is the acoustic wavenumber and a is the active radius of the transducer.[23] The approximate active radius of the Signature1000 echosounder is 15 mm. For the nominal sound speed of 1500 m/s, this yields $\Psi = -28.34$ dB re 1 steradian. Lacking measurements to calculate Ψ, here we assume that Equation 9 predicts the equivalent beam angle adequately. Given the k term in the denominator, the equivalent beam angle theoretically follows a f^{-2} dependence. Furthermore, this indicates that Ψ is dependent on the sound speed and should be calculated given local conditions rather than the nominal value.

Transducers with large bandwidths can, therefore, have significant variability in Ψ as a function of frequency. An equivalent beam angle represented by the linear mean of $\Psi(k)$ across the transmitted bandwidth is implemented. For example, $\Psi = -28.27$ dB re 1 steradian for $c = 1500$ m/s when averaged across the full bandwidth. During Lake Washington tests the sound speed was approximately 1482 m/s resulting in $\Psi = -28.38$ dB re 1 steradian over the full bandwidth. Here, we have accounted for both the sound speed and bandwidth impacts. Overall the impacts of the sound speed on Ψ are on the order of a few tenths of a dB or less. The equivalent beam angle combined with the range resolution, dR, represents the ensonified volume at range R and is implemented as described in Equation 3. The equivalent beam angle and range resolution are not relevant in the calculation of the Target Strength, which assumes the presence of a single, small scatterer within the beam.

Ideally Ψ is determined using measurements as opposed to the approximation described above. To do so, the calibration target is suspended below the transducer and swept through the beam to map out the two-way angular dependence of the beam.[12] This, however, requires an experimental apparatus capable of suspending and manipulating the sphere precisely in a suitable environment at a sufficiently large range such that the sphere only occupies a relatively small portion of the beam volume. Thus, a large tank is required. Relatively few facilities with existing experimental apparatuses to perform these measurements exist, making the approximation of the two-way equivalent beam angle the most practical approach despite the added uncertainty.

The final term implemented in both the TS and S_v equations are the calibration gains (G or G_{int}). These values are ultimately determined in calibration, which is described in detail in the following section.

4 CALIBRATION: BACKGROUND, MEASUREMENTS, AND PROCESSING

The calibration process is broken into three parts. The first describes two approaches to sphere calibrations and a theoretical target strength calculation to establish gain values. Next, we describe the calibration measurements, which were performed by suspending spheres below SWIFT drifters in Lake Washington, WA. The third subsection describes the post-processing used to calculate the gain. If unfamiliar with general echosounder calibration procedures, please see Demer et al.[12] and references therein, which provide additional details including how to prepare and suspend calibration spheres.

4.1 High-frequency calibrations

The purpose of calibrating an echosounder is to facilitate the conversion of the signals received by transducers, and processed by their associated system components, into quantitative values. Historically, calibrated echosounders are used for acoustic-trawl surveys and to support studies of backscattering by marine animals. In these applications, results of integrated backscattering measurements are combined with representative backscatter from animals and survey area size to estimate abundance.[9] As a result, common echosounder calibration procedures have been developed to minimize potential biases. Echosounders consist of numerous components that would require independent calibration across a range of potential operational parameters, some of which cannot be replicated in many laboratories. Therefore, the most common approach to calibration involves the use of spheres suspended below the transducer using thin monofilament line, which are recorded and processed using the SONAR equation.[9–11;31] There are analytical solutions for the acoustic backscattering from a sphere whose material properties are known.[15] By inserting this term on one side of the SONAR equation, the user solves for the system's calibration gain, which accounts for factors affecting the system's operation. While systems have evolved and subtle differences in calibration have been adopted as technology has advanced[11–13;17;31–33], overall calibration procedures have not evolved significantly in recent decades.

Although they share some similarities, there are multiple ways to approach calibration using spheres depending on the transit signal parameters and sphere properties. These include total scattering (*full wave*) and *partial wave* methods, with the main difference being that the partial wave approach relies on separating the echo off the front interface of the sphere from the signals associated with circumferential waves and resonances.[10;16] To do so, this method requires a relatively large sphere and high temporal resolution, typically achieved through pulse compression of frequency modulated signals with large bandwidths. Here, we adopt the full wave solution that can be applied to both continuous wave or frequency-modulated pulses with modest sphere sizes. However, we include a discussion of the partial wave calibration because it has benefits for calibrating systems like the Signature1000.

All sphere calibrations are dependent on a model for the target strength of the sphere used. The target strength as a function of frequency for an elastic sphere has a complex dependence on frequency. This relationship, which is used in the full wave calibration approach applied here, is shown for a 38.1-mm diameter tungsten-carbide sphere with 6% cobalt binder (referred to as WC38; Figure 1) across a broad range of frequencies. Ideally, calibration is performed in the frequency range where $TS(f)$ varies smoothly while avoiding the Rayleigh scattering regime at relatively low frequencies.[12] This ideal range corresponds to approximately $1 < ka < 10$. For the WC38 sphere this ideal calibration range corresponds to frequencies 10–75 kHz, which is more than one order of magnitude below the Signature1000's operational frequency. For such high operational frequencies, typical sphere calibrations are impractical because sphere diameters less than ∼5 mm would be required to operate in the portion of the curve where the response is smooth. Such a target would have a much weaker TS and also be subject to larger bias due to scattering from the monofilament line used to suspend the sphere.[34]

Using the full wave approach the theoretical, average TS for the sphere over the transmitted bandwidth can be substituted into the various equations in Section 2 to calculate the calibration gain. This can be applied in both point scattering applications simply by rearranging Equation 1b to solve for G and inserting the theoretical value. In applications focused on volume backscatter, the mean TS over the bandwidth is used in Equations 3, 6, and 7, which is the method adopted here. More details describing these calculations and post-processing using this approach are included in Section 4.3. The partial wave equation is typically used to calculate the gain using Equation 1b, which can be applied in volume scattering applications with modifications to the S_v equations.[5;17;20;33]

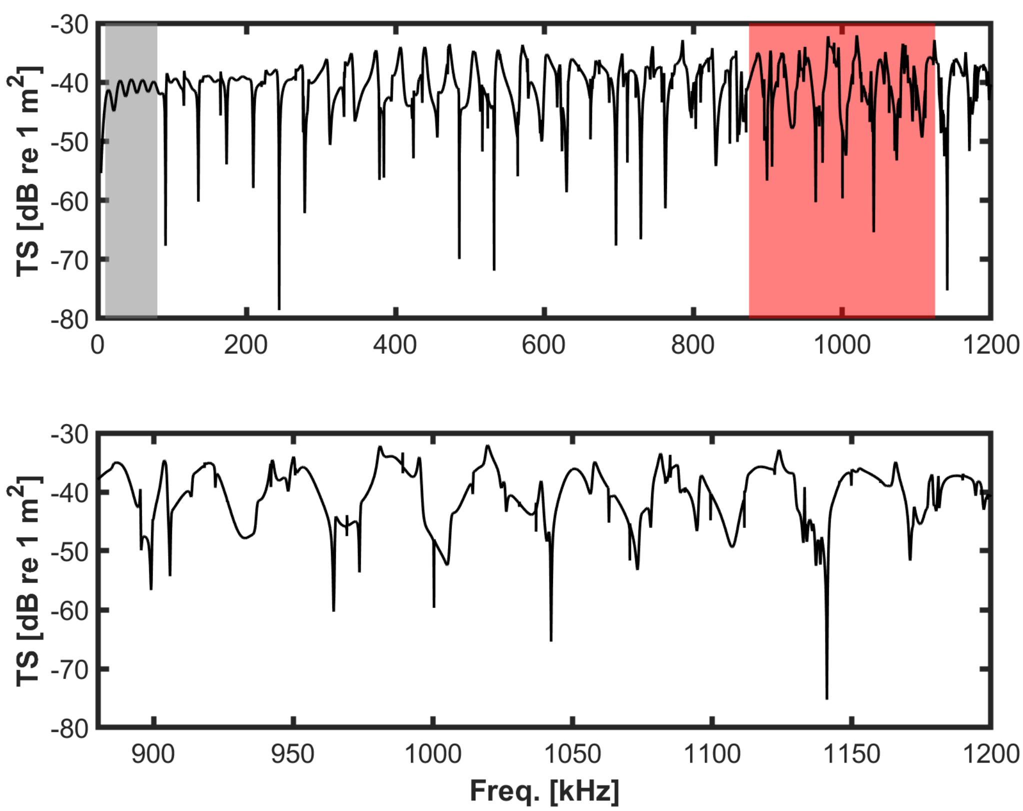

Figure 1: (top) The frequency-dependent target strength of a 38.1 mm diameter tungsten-carbide sphere with 6% cobalt binder from 5 to 1200 kHz. The gray area highlights frequencies where the response from the WC38 is "well-behaved" while the red area highlights the high frequencies relevant here. (bottom) The target strength curve spans the high frequencies at which the Nortek Signature1000 operates.

In addition to these considerations, the operational settings of the echosounder play a role

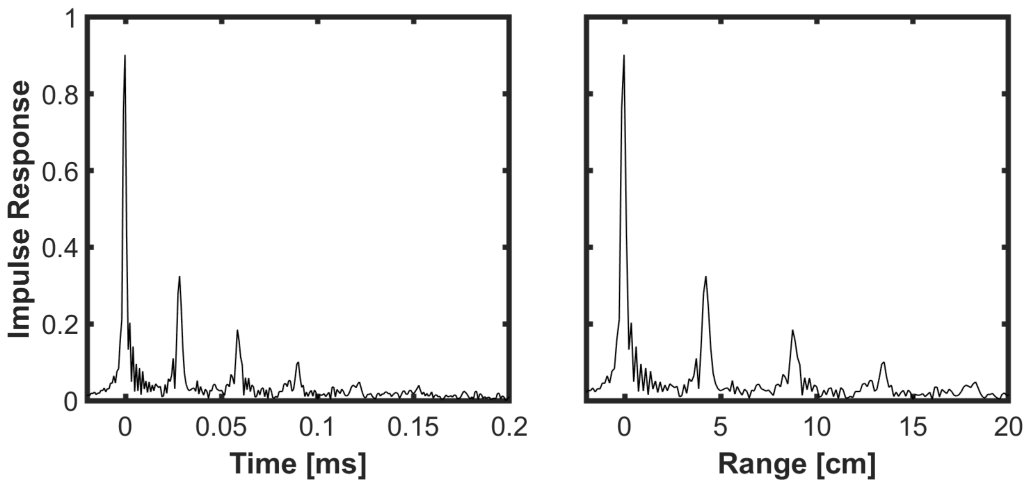

Figure 2: The impulse response of the WC38, calculated as a function of time (left) and inferred range (right), assuming a sound speed of 1500 m/s. The latter is used because it is more easily coupled to the standard range outputs of the Signature1000 echosounders. Both panels show the response from the front interface centered at x=0.

in calibration. Even when operating at high ka values, an alternative approach that avoids the challenges of the complex sphere response is possible if a broadband signal with a large bandwidth is used. Through pulse compression, such signals can achieve the range resolution required to isolate the scattering from the front interface of the sphere.[16;19;35] By doing so the partial wave approach avoids the complexities of the full wave solution that are highly dependent on the sphere's properties[10;16] (Fig. 1).

In the case of the Nortek Signature1000, the transmitted bandwidth is approximately 250 kHz and the theoretical range resolution of pulse-compressed signals is $\Delta r = \frac{c}{2BW}$, where BW is the transmitted bandwidth and c is the sound speed.[16;19;28] Thus, the Signature1000's theoretical range resolution, assuming a sound speed of 1500 m/s, is approximately 6 mm, although this value is not generally achieved due to tapering and other non-ideal aspects of the transmitted signal. The impulse response for a WC38 sphere (Fig. 2) shows that the echoes associated with the front interface and first circumferential wave are separated by approximately 0.028 ms (or 4.2 cm using 1500 m/s). Thus, the partial wave calibration approach could be used with the Nortek Signature1000 echosounders and WC38 spheres if raw signals are recorded.

For the partial wave calibration, valid when $ka \gg 1$, where a is the sphere radius and k is the acoustic wavenumber, the backscattering amplitude is described by

$$F \simeq \frac{1}{2} a \mathscr{R} e^{2ika}, \tag{10}$$

where $\mathscr{R} = (gh-1)/(gh+1)$, $g = \rho_s/\rho_w$, $h = c_s/c_w$, and the subscripts refer to the properties of the sphere and water, respectively.[16] Note that c_s refers to the compressional wave speed of the sphere. This is converted to the partial wave target strength according to $TS = 10\log_{10}(|F|^2)$. SWIFTs do not record raw, pulse-compressed time series so a partial wave calibration is not possible. However, this approach is useful and could be further facilitated by using larger spheres (e.g., diameters greater than 38.1 mm). To carry out such a calibration the theoretical partial wave TS would be

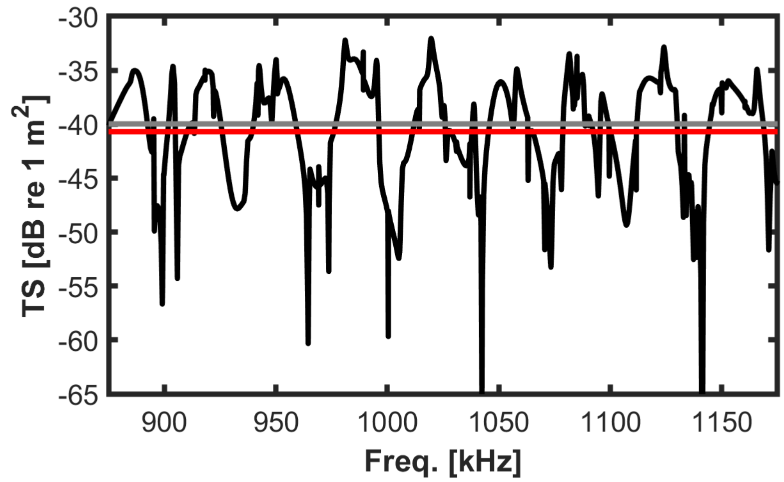

Figure 3: The full wave TS of a WC38 sphere over the bandwidth of the frequency modulated Signature1000 transmit signal. The grey line shows the average TS of the full wave solution over the band, and the red the TS corresponding to the partial wave solution.

applied to Equation 1b to solve for G and used in point scattering applications. When applied to volume scattering, an effective pulse duration could be used to calculate a further offset to produce a total gain term similar to G_{int} that accounts for the pulse compression. Further details are beyond the scope of this report but are available in numerous references.[16;20;33]

Because either the full wave or partial wave methods can be used in calibration, the differences in the average target strength across the band from these results are worth considering. Figure 3 shows an example of the theoretical TS across the band of the Signature1000 echosounder and the average target strength associated with the full and partial wave solutions. The partial wave solution yields $TS = -40.7$ dB re 1 m^2, and the full wave approximately –40.0 dB re 1 m^2. Given that the true material properties are unknown and the theoretical backscattering cross-section is highly sensitive to them, there are larger uncertainties related to high ka calibrations using the full wave approach. In any calibration, it is best practice to calculate the theoretical target strength using local water properties.

4.2 Field measurements

To calibrate the Nortek Signature1000 series echosounders six 4$^{\text{th}}$ generation SWIFT drifters[2] (buoy numbers 22–26 and 28) were rigged to replicate the on-axis calibration methods described in Demer et al.[12] by integrating the sphere echo. First, 38.1-mm tungsten carbide spheres with 6% cobalt binder were tied into harnesses with long end loops allowing them to be girth hitched to a bridle (Figures 4 and 5). Each SWIFT contains multiple feet with small holes to which anodes and other ancillary equipment are fastened during deployments. A two-point monofilament bridle, each end terminated with overhand knots on bites, was shackled to two of the legs with the sphere suspended in the middle. All rigging was performed using 0.51-mm Berkley Trilene monofilament (30 lb. test). At approximately 6 m, the width ensonified by the full beam (2.9° at the center frequency) is approximately 30 cm. Note, however, that with the use of the broadband pulses the beamwidth is much narrower at the upper end of the frequency bandwidth. As a result, the impact

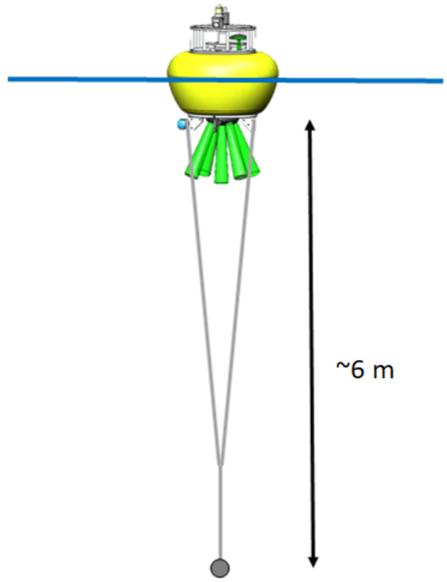

Figure 4: A drawing of a 4th generation SWIFT drifter with a bridle and calibration sphere suspended below it. The targeted sphere suspension range was approximately 6 m. The sphere is sufficiently heavy that in an environment with no currents, an additional weight suspended below the sphere was not necessary.

of the beamwidth on targets just a few centimeters off axis at the shorter ranges can be significant. For these reasons, relatively large suspension ranges are recommended, although these must be balanced against the operational range limitations of the high-frequency units. Thus, a range of less than 10 m was chosen.

Calibration of the six SWIFTs was performed on 28 June 2023 on Lake Washington. Throughout the operations winds were out of the south at less than 5 knots, resulting in relatively small waves. Skies were clear throughout the day. While drifting the sphere hangs freely and the motion of the SWIFTs in response to the surface waves causes the sphere to “swing” throughout the beam. For reference, calibration measurements were also made in April 2023 under modestly windier conditions but the SWIFT motion was found to be significant enough that the overall number of targets likely within the beam was much lower so the measurements were repeated.

Three spheres and sets of bridles were available for the June 2023 calibrations so the SWIFTs were deployed in groups of three. To avoid fouling the bridle, each unit was lowered into the water sphere first and released. The vessel then moved at least 50 m away before deploying the next SWIFT (Fig. 5). Once all three units were in the water the vessel moved to distances greater than 1 km from the SWIFTS to perform other work and returned to recovery the units after a minimum of 75 minutes. The units were then recovered, the bridles and spheres swapped to the three remaining SWIFTS, and the process repeated.

The goal of this work is to characterize the SWIFTs not as they might hypothetically be used, but rather as they are regularly used by researchers at the Applied Physics Laboratory at the University of Washington. Thus, we maintained all of the default settings used in normal data acquisition. The standard SWIFT duty cycle is to operate for 512 s then enter a 208-s period for processing and telemetry before repeating. In total, more than 14,000 active pings were available

Figure 5: (left) A picture of three SWIFTS equipped with spheres drifting in Lake Washington. (right) A SWIFT with the ∼6-m bridle attached to a sphere prior to deployment in Lake Washington.

for processing from each of the individual SWIFT deployments. Following recovery, data files were processed (Sec. 4.3) to determine individual gains for the units and to generate post-processing scripts to serve as methods to calibrate the Signature1000 echosounders on SWIFTs.

A profiling buoy (https://green2.kingcounty.gov/lake-buoy/) determined a temperature profile to calculate the sound speed (Fig. 6) in the upper 7 m of the water column and to calculate the mean sound speed to correct the Signature units' nominal sound speed and to estimate attenuation rates. We note that elevated scattering in the water column was consistent with measurements of the thermocline and profiles identified peaks in chlorophyll in the upper 10 m of the water column.

4.3 Processing calibration data

Given the SWIFT output data format, the approach to calibration is similar to the methods described in Sections 2 and 3 and in other documents for volume scattering measurements.[12;32] Specifically, the signal recorded by the SWIFTS represents the average pulse compressed power over pre-determined range bins, which precludes a frequency-domain analysis of the signals. The calibration method applied to the Signature1000 echosounders herein assumes that the time-domain signals are consistent with the analytical frequency-domain solution. Therefore, the average TS across the transmitted bandwidth (-40.0 dB re 1/m^2) is used in calibration. The calibration is performed following Equation 7 using the steps described below.

Step 1: Individual ADCP files are pre-processed to consolidate all relevant measurements into one file that includes a range vector and an array including all of the echosounder pings. All data associated with periods during which the units are not operating are removed from the time series (e.g., the ADCP was removed from the water or the sphere was not present). In addition, periods where fish or other obvious targets are in the vicinity of the sphere are removed. Lastly, if discrete

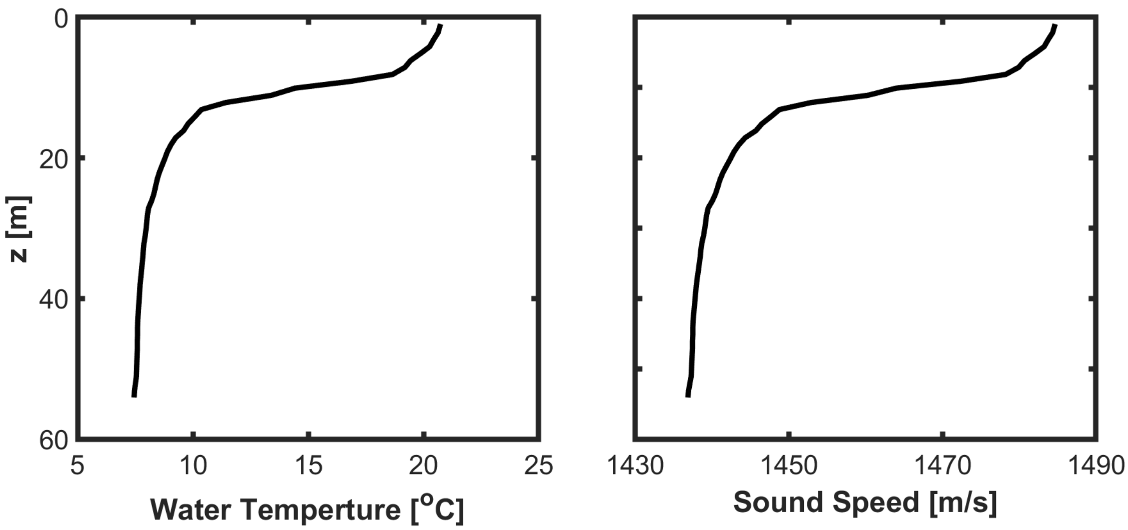

Figure 6: Temperature and sound speed profiles from calibration drifts using the SWIFTs on 28 June 2023. While significant stratification is observed at depth, the upper 7 m, where the tests were carried out, exhibited more limited gradients of temperature and sound speed. The mean temperature and sound speeds in this layer were approximately 20°C and 1482 m/s, respectively.

events such as bubble plumes contribute significantly to scattering in the upper water column, the data were removed.

Further review for quality control is also done at this stage. If the sphere is the only regularly observed target it should be clear at the expected range. In the case of SWIFT measurements, the target may drift rapidly in and out of the beam due to platform motion. However, targets that move within the water column in close proximity to the sphere are not uncommon. Figure 7 shows one such example in which the target is clear but another target (likely a fish) appears in close proximity to the target on a regular basis. Pings contaminated by additional targets in close proximity to the sphere should to removed prior to further processing. Close proximity is ultimately dependent on the transmitted bandwidth, whether or not pulse compression is used, and the relative strength of the targets.[13] However, a cautious guideline would be to remove any pings with additional targets appearing within the range of $c\tau/2$ of the sphere, where τ is the pulse duration. Adopting this approach ensures that signals from adjacent targets will not overlap regardless of whether narrowband or broadband pulses are used. This may not be possible in data sets with high levels of contamination from other targets. In those cases, it is worth performing the measurements again, if possible.

Step 2: Assuming the sphere has a fixed harness length the sphere's apparent location can shift in the water column based on the off-axis angle, but will fall within a limited set of range bins given the beam pattern. Thus, by manually reviewing data with knowledge of the harness length one can readily "search" for the sphere over a limited set of indices corresponding to the expected range from the transducer. Figure 8 shows a series of 1000 consecutive pings in the upper 10 m of the water column. In this case, the sphere is located at approximately 6.1 m. At this stage, the range vector is used to find indices corresponding to the expected location of the sphere to be used in the subsequent processing steps. Here, a set of values corresponding to ± 0.5 m is used arbitrarily. If additional targets are present within the range of the sphere, that further restriction

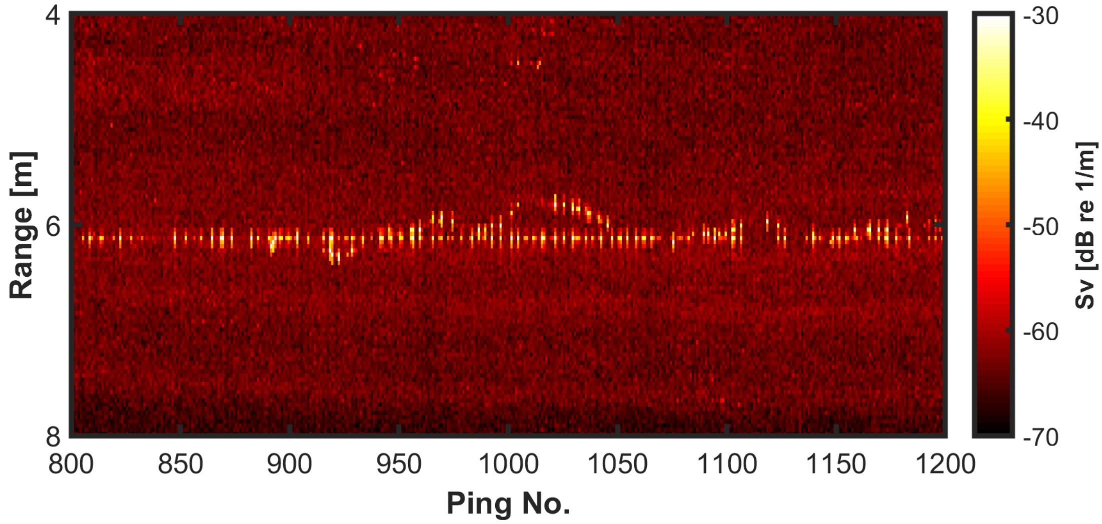

[!h]

Figure 7: An echogram of the WC38 sphere at approximately 6.1 m during measurements with SWIFT buoy number 24. Prior to ping 900 the variability in the target is driven by the SWIFT's motion. In the middle of the echogram (pings 900 to 1050) a second target, probably a fish, appears around the sphere. Where echoes from the targets overlap and are included in the analysis the final calibration may be biased.

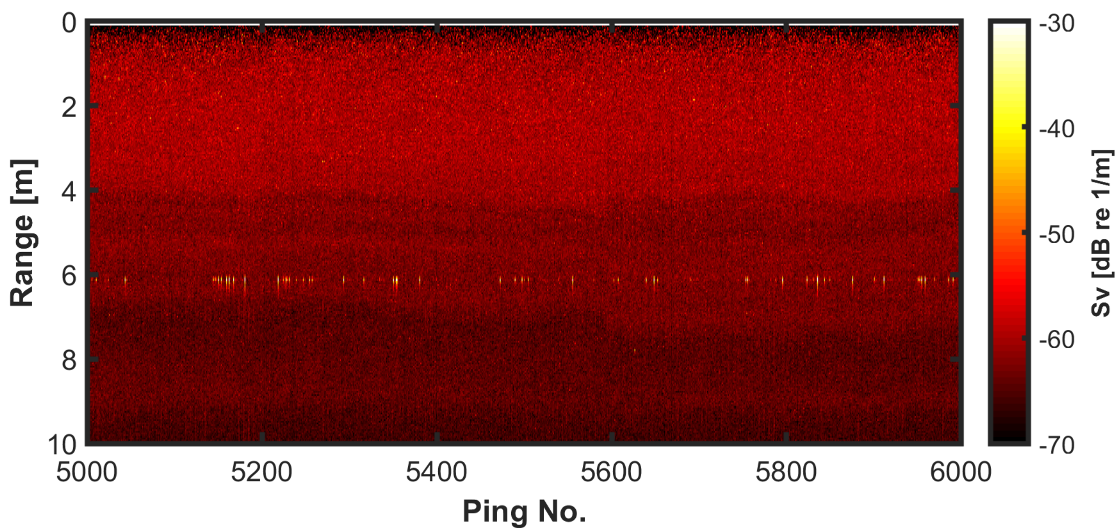

Figure 8: An example echogram, calculated post calibration, showing S_v during one of the calibration drifts. The sphere is located at approximately 6 m and its movement in and out of the beam is obvious. The layers of stronger and weaker scattering elsewhere in the water column are likely attributed to the thermocline and other scatterers including plankton or suspended particulate.

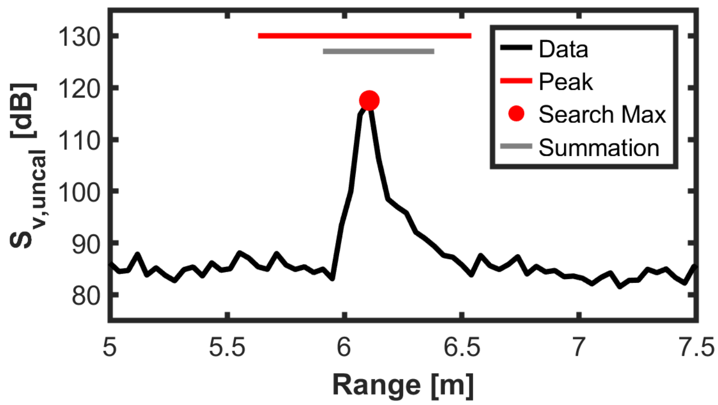

Figure 9: An example of the Nortek Signature1000 output for a sphere using nominal range bins of 4 cm. The red line shows the range bins searched to identify the peak echo intensity while the red dot shows the range of the peak. The grey line shows the portion of the signal over which the summation is performed to in calculating G_{int}.

of indices may be warranted.

Step 3: Once the expected range to the sphere is established, $S_{v,uncal}$ is calculated for all pings and ranges by solving Equation 3 neglecting the G_{int} term using the various values described in Section 3. For each ping, the index corresponding to maximum echo intensity within the range window is identified. An example ping showing the $S_{v,uncal}$ signal is included in Figure 9 with annotations showing this process. Note this figure also includes annotations associated with subsequent processing steps. The sum of $10^{S_{v,uncal}/10}$ values over a window spanning 20 cm before to 27 cm after the peak echo intensity is calculated and represents the integrand in Equation 5. Asymmetry in this window is driven by the pulse compression and the extended echo caused by the sphere properties. This window contains nearly all of the energy from the echo (Fig. 9) and is adequate to resolve a sphere's frequency-domain response.[13;17] The summation is converted to s_a by multiplying the value by the total thickness of the layer over which the summation was performed (final term is Eq. 7).

Step 4: With the theoretical target strength of the sphere (here calculated to be TS= –40.0 dB re 1 m^2), beam parameters, and $s_{a,uncal}$ calculated from $S_{v,uncal}$, the final calibration values can be solved according to Equation 7. However, at this point, it is necessary to consider the operational limitations of the unit for the final calculations. If the units were split aperture, thereby allowing the target to be located within the beam, the path forward would be clear: select the targets known to be on-axis. Without this, a more ad hoc approach must be adopted. Because the beam is quite narrow, the intensity associated with the strongest echo may be the best measurement of the on-axis response. Using a single ping, however, may bias the results if other targets are in the vicinity of the sphere. After removing any pings likely contaminated by scattering from other sources, the approach adopted here is to sort the received intensity values and select three sets of data:

- The value associated with the highest intensity echo
- The values associated with the five strongest echoes
- The values associated with the 10 strongest echoes

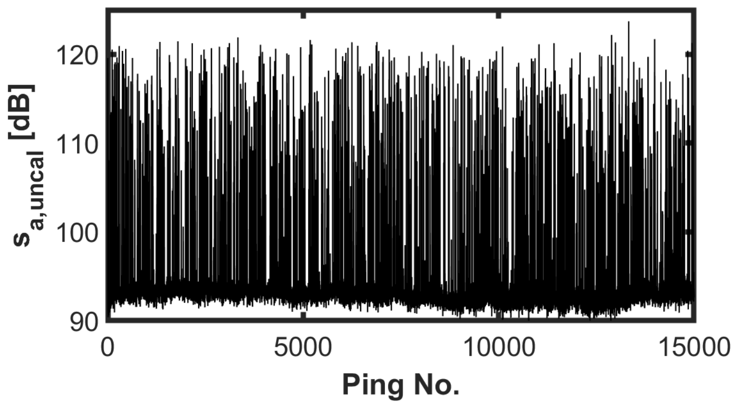

Figure 10: Values of $s_{a,uncal}$ for pings during one SWIFT calibration. The rapid changes in P_r are attributed to the motion of the SWIFT that causes the sphere to move in and out of the beam. The ping corresponding to the highest measured value (~125 dB; near ping number 13500) was reviewed and is attributed to a fish. Such pings are removed before calculating G_{int}.

All of these are used to derive final calibration values using the different numbers of targets, allowing for comparisons between the values. The data here include more than 14,000 individual pings. The use of a small number of targets ultimately reflects the high level of variability in the measured echo intensity due to the small beamwidth and significant motion of the SWIFTs (Figure 10). The thresholding decisions made here are arbitrary and other choices may be preferable, particular using platforms more stable than the SWIFT.

Step 5: The final step is to aggregate the $s_{a,uncal}$ values for targets selected in step 4, take their averages, and solve for G_{int}. Thus, for cases with multiple pings to average, Equation 7 becomes

$$G_{int} = 10\log_{10}\left(\frac{10^{TS_{th}/10}}{10^{\Psi/10}\ r_s^2}\right) - 10\log_{10}\left(\frac{1}{m}\sum_{j=1}^{j=m}\left(\sum_{i=min\ R}^{i=max\ R} 10^{(S_{v,uncal}(R_i))/10}\right)\Delta R\right), \tag{11}$$

where j is an index associated with the targets selected for the final calibration calculations and m is the total number (e.g., 1, 5, or 10 if using the approach described in step 4).

Step 5 yields the final calibration values determined by the integration of targets determined to be roughly on-axis. This value can be applied in the S_v equations to process data and one value is obtained by this process for each buoy number tested. In the processing scripts there is a flag that allows use of the average value across all calibrated units or the specific value of a SWIFT buoy number/ADCP.

5 RESULTS

Calibration gains are presented in this section for all six SWIFTs deployed on Lake Washington in June 2023. SWIFT buoy number 24 had a high degree of contamination from targets believed to be fish. These pings, as with similar scattering from other units, were removed from the analysis. This resulted in nearly 50% fewer pings available for this unit. Nonetheless, we have chosen to include the results here because the remaining pings resulted in gain values comparable to those derived from the other units.

The results from the integration calibrations for G_{int} are shown in Table 1. Depending on the unit, the gain value corresponding to a single ping believed to be attributable solely to the sphere following quality control steps was between 0.3 to 1.7 dB larger than averages corresponding to the top five pings. Differences corresponding to the average of the top ten pings versus the single varied by as little as 0.7 dB to greater than 3 dB. If all of the targets included in this limited analysis were located roughly on-axis, a smaller degree of variability in gain values would be expected. This is likely attributed to challenges associated with capturing targets on-axis in field measurements where precision instrumentation is unavailable and the transducer's beamwidth is narrow. Lacking further information to justify the use of a specific gain value from Table 1 we proceed by applying the gain value calculated from the five highest intensity pings following the removal of pings clearly contaminated by other targets. This decision is arbitrary but well-justified given the relatively small number of high-intensity targets indicating that the sphere was on-axis.

The gain estimates (Table 1) vary by 3.5 dB across the six calibrated units. The degree to which these values are driven by real differences between the transducers versus imperfections in the sampling process and calibration cannot be determined. Furthermore, there are no suitable references for precision calibrations of numerous Signature1000 echosounder units available for comparison. However, calibrations of numerous Nortek Signature 100 units have been made in a tank.[21] While the methods vary slightly from those discussed here, the underlying principles are the same. The measurements of numerous Signature 100 echosounders showed variability consistent with the measurements here [personal communication, George Cutter (NOAA Fisheries)] and suggests that variability between units could easily explain the differences in calibration estimated in this study.

For comparison, on-axis gain (G) calibrations based on only the peak value of the measured signal using Equation 1b with the partial wave calibration target strength ($TS = -40.7$ dB re m^2) are provided here. *These values are provided for context but this approach cannot be applied without further corrections due to the averaging.* Here, we describe the impact of this range correction and

Table 1: Calibration gain estimates using different numbers of targets for all six Nortek Signature1000 units installed on the SWIFTs.

Date	Range [m]	Buoy Number	$G_{int,1}$ [dB]	$G_{int,5}$ [dB]	$G_{int,10}$ [dB]
28 June 2023	6.02	22	–150.7	–149.0	–147.5
28 June 2023	6.18	23	–150.4	–149.4	–148.2
28 June 2023	6.1	24	–152.5	–152.2	–151.8
28 June 2023	6.1	25	–149.5	–149.1	–148.8
28 June 2023	6.02	26	–152.4	–152.0	–151.6
28 June 2023	6.18	28	–149.0	–147.6	–147.7

Table 2: Calibration gain using the partial wave target strength value without compensating for the impacts of averaging across the range bin. These values are biased low due to processing uncertainties so these values should not be applied directly. They are presented for the purpose of discussion.

Date	Range [m]	Buoy Number	G_1 [dB]	G_5 [dB]	G_1 [dB]
28 June 2023	6.02	22	–139.6	–138.4	–137.0
28 June 2023	6.18	23	–138.6	–137.8	–136.8
28 June 2023	6.1	24	–141.8	–141.5	–141.1
28 June 2023	6.1	25	–138.5	–137.9	–138.5
28 June 2023	6.02	26	–141.1	–140.8	–140.3
28 June 2023	6.18	28	–137.5	–136.5	–135.5

implications for comparisons with the gain values from integration in Table 1.

Calibration results for G_{int} and G vary approximately 11–12 dB. This variability is expected given the averaging performed by the units prior to recording the data in 4-cm range bins. The impact of this can be considered by modeling the time-domain response of the sphere and comparing the output that would be used in a typical calibration to the one recorded with the settings used by the SWIFTs. To do this we create a signal that represents the envelope-squared of the convolution of the sphere's impulse response with the transmitted signal (875–1125 kHz; no taper; 0.1-ms duration). This approach assumes that the theoretical TS curve is accurate and the transmitted signal and receive sensitivities of the unit are flat across the bandwidth. Neither of these assumptions is well-justified, but in the absence of measurements, the exercise is still valuable. Next, the normalized envelope-squared is averaged over 4-cm windows to produce a value representing the bin-averaging. This is repeated by moving the center of each bin in 0.1-cm increments to show how this averaging would impact measured signals relative to a modeled, theoretical signal. These examples are shown in Figure 11 and clearly reveal the impacts of the range bins. Notably, there is a difference of approximately 7–10 dB between the full-resolution signal and the signals averaged with a resolution of 4 cm. The magnitude of this difference is dependent on where the sphere is located within the range bins. This is to be expected and explains most of the difference between the G and G_{int}. If working with data averaged in a comparable way, on-axis gains could be calculated by offsetting the G values by the impact of this averaging plus the s_a correction[12] or effective pulse duration. If properly carried out, $G_{int} = G + G_o$, where G_o is a placeholder representing the various terms (e.g., averaging, pulse form) not explicitly calculated here.

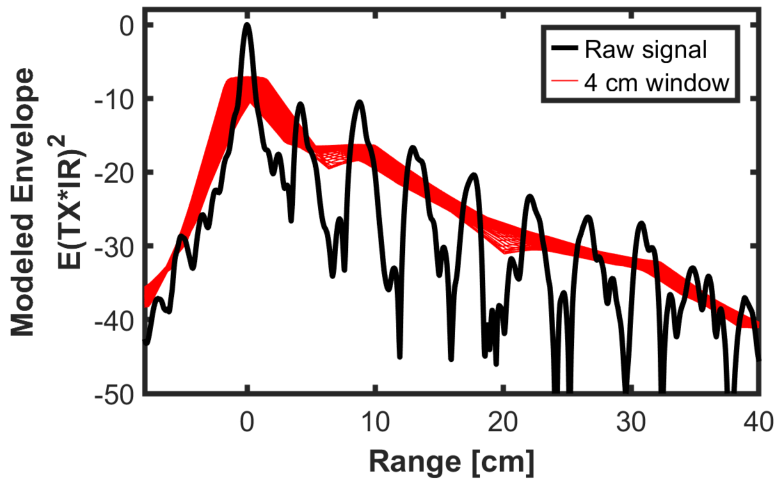

Figure 11: Examples of normalized time-domain responses simulated from a WC38 sphere's impulse response and the transmitted signal. The x-axis simulates range, as is standard in an echogram, corresponding to the time delay, which is set to zero at the front interface of the sphere. The black curve shows the response expected from a raw signal, which could be used with a spatial wave or standard, frequency-dependent broadband calibration. The red curves show the response averaged in 4-cm windows centered in positions iterated in 0.1-cm increments to bound the impact of averaging on measured signals. Note that the peak is nearly 10 dB lower in the average curve and slowly rolls off in time without revealing the complex peaks associated with resonance and circumferential waves.

5.1 Uncertainties and limitations

There are too many uncertainties to calculate a detailed uncertainty budget, but it is worth considering the magnitude (and sign) of probable impacts. The three most significant sources of uncertainty are related to the properties of the sphere itself, the actual position of the sphere in the pings used to calculate the calibration gain, and additional scattering associated with the bridle.

The calibration gains determined from the integration of the uncalibrated volume backscattering are sensitive to the full wave response of the sphere over the integrated range bins. As a result the uncertainties regarding the material properties, specifically the density and sound speed of the sphere, are important. At high ka values the sphere response is complicated and some disagreement between the resolved frequency response and theory is to be expected. In practice, the TS of the sphere averaged over the bandwidth of the transmitted signal could be greater than or less than the predicted value. There is, unfortunately, no simple method for determining this unless a material likely to have a high purity (e.g., a copper sphere) is used. The most practical approach for reducing this uncertainty in the future is to perform a partial wave calibration. Doing so would benefit from the use of a larger sphere (e.g., a 60-mm copper sphere) in addition to performing the calibration using the raw data format. Thus, a standard, on-axis calibration using the TS equation could be applied and a term, often referred to as the $s_{a,corr}$, could be applied for processing S_v measurements.

The most significant uncertainty is likely associated with the position of the sphere within the beam during calibration. Here, the general assumption is that the targets used to calibrate the gains are located on the axis of the beam. The variability in gain values between the values calculated with an individual target and ten targets alone suggests that this is extremely difficult to achieve without precision testing facilities. Because the beam is so narrow, –3 dB at less than 1.5° at the center frequency and much narrower at higher frequencies, offsets on the order of centimeters from the center of the beam can have notable significant impacts on the calibration gains. While we are confident that the targets analyzed for the calibrations were located within the beam, we cannot effectively bound the total impact on the calibration. It is not unreasonable to assume that if the sphere was indeed located well within the beam at the center frequency that the total uncertainty of the calibration would be on the order of 3 dB or less. For targets slightly off-axis the measured backscattering intensity would be modestly less than the idealized value while the calibration equations assume the target is on-axis. Thus, a lower gain value (i.e., a less negative number) would be derived from these circumstances.

The impact of sphere suspension is also unknown but cannot be neglected. Its magnitude is likely to be smaller than those associated with the TS of the sphere and the sphere's position within the beam. The practical impacts of the harness and bridle are derived from their contributions to the total scattering within the integrated window. Given the high frequency of the Signature1000 echosounder one would reasonably expect that both the contributions of the monofilament and the additional uncertainty associated with it would be much larger than units operating at lower frequencies.[34] Because the operational frequencies are fixed, this is unavoidable. To reduce this uncertainty to the greatest extent possible it is best to use relatively thin monofilament for sphere suspension to ensure that large knots where different components of the bridle meet are located outside of the windows of data used for analysis. This can also be mitigated through the use of a higher target strength sphere.

Full wave calibrations to calculate G can be performed but were not the focus here as the processes of interest in most SWIFT applications are typically associated with volume scattering. Furthermore, the pulse compression and averaging in the data, as acquired, increase the uncertainty of such a calibration. Nonetheless, here we have provided approximate calibration values corresponding to the partial wave calibration with the caveat that the averaging that occurs over the windows increases the uncertainty. This approach is not generally recommended and was simply provided here for context and comparison. In the future on-axis TS measurements using the partial wave method to estimate gains would benefit from the system operated in FM (broadband) mode with raw signals and larger spheres. This combination of choices would make it easier to isolate the sphere's response and apply the partial wave calibration methods used in other studies.[10;12;16;35] Because of the high temporal resolution of the pulse-compressed signals (i.e., ∼6 mm, in theory), this does not require the large spheres to be used as is required with low-frequency systems. In fact, the spheres similar to the WC38 used here should be sufficient. Modestly larger spheres would simplify the procedure by providing longer time delays between the echoes from the sphere's front interface and circumferential waves and resonances.

To mitigate these uncertainties tank measurements are the easiest and most effective way to perform such calibrations. Of course, this requires additional resources and testing infrastructure that can facilitate cm-scale precision in measurements. Alternatively, one could deploy the Signature series echosounders adjacent to a split-beam echosounder. This would allow the position from the split-beam echosounder to be used to map the sphere's location by ping to better constrain the uncertainties in the single-beam analysis.

The methods presented here are imperfect but represent a reasonable effort to operate and calibrate the Signature1000 echosounders when facilities, time, and budgets are limited. We think the calibrations likely have uncertainties on the order of ± 3 dB, although it is possible that they are larger. Such uncertainties would be unacceptable in applications like fisheries acoustics where they would be associated with ±50% uncertainties in relative abundance. However, in most oceanographic applications the broad impact of these uncertainties is less important. In fact, the alternative to using the systems without calibration is that the systems produce relative intensity values that cannot be related quantitatively to scattering processes and models. Using calibrations, despite the uncertainties, has clear benefits for both quantitative and qualitative measurements using the Nortek Signature series echosounders.

6 NOISE ESTIMATES AND CORRECTIONS FOR GENERAL PROCESSING

The equations for S_v and TS, as defined in Section 2 (Equations 1a and 1b), do not included the term for noise threshold included in Nortek's documentation. This term is often included in echosounder processing and is particularly important when echoes are being integrated or the system is operating near the noise floor. This is true whether the noise is driven by the system itself, other acoustic/electrical interference, or ambient noise. The equations, modified to include a noise correction term are

$$S_v = 10\log_{10}\left(10^{P_r/10} - 10^{NT/10}\right) + 20\log_{10} R + 2\alpha R + PL - 10\log_{10}\left(\frac{c\tau}{2}\right) - \Psi + G_{int}, \text{and} \tag{12a}$$

$$TS = 10\log_{10}\left(10^{P_r/10} - 10^{NT/10}\right) + 40\log_{10} R + 2\alpha R + PL + G + B(\theta), \tag{12b}$$

where NT is the measured noise threshold (in dB). Correction for noise is not always necessary. For example, if the sampled depth ranges have high levels of backscattering then the signal to noise ratio (SNR) may be high enough that the impact of a noise correction is minimal. However, when the signal to noise ratio is low or the echosounder is operated to ranges where there are no longer clear signals from scattering, removal of the noise will improve the quality of the echograms and limit the potential for attributing observations to scattering instead of noise.

Because NT is driven by many factors it should be estimated regularly to properly account for it. Because noise and scattering levels will vary in different situations, a single script cannot be prepared that will estimate accurately a noise floor for general use. We approach this problem by providing a detailed summary of how the the NT was calculated for the calibration data sets. Assuming this is representative of the system's noise floor and that other sources of noise would only increase the noise level, this threshold has been integrated into the processing scripts for noise removal. This term, however, should be revisited to confirm this assumption or to modify the threshold if it is found to be significantly different in other environments.

One simple and common approach to establishing the noise threshold is described by De Robertis and Higgenbottom (2007).[36] This is the method adapted for the Signature1000 processing. Although it is possible to work directly with Equations 12a and 12b, the approach used here is similar mathematically, but is carried out in multiple steps not detailed in those equations. This includes identifying periods in the data believed to be representative of the noise floor, inserting the noise threshold into the general S_v equation in place of P_r, calculating a corrected S_v term with the noise subtracted, and finally setting basic thresholds to remove data points with low SNR.

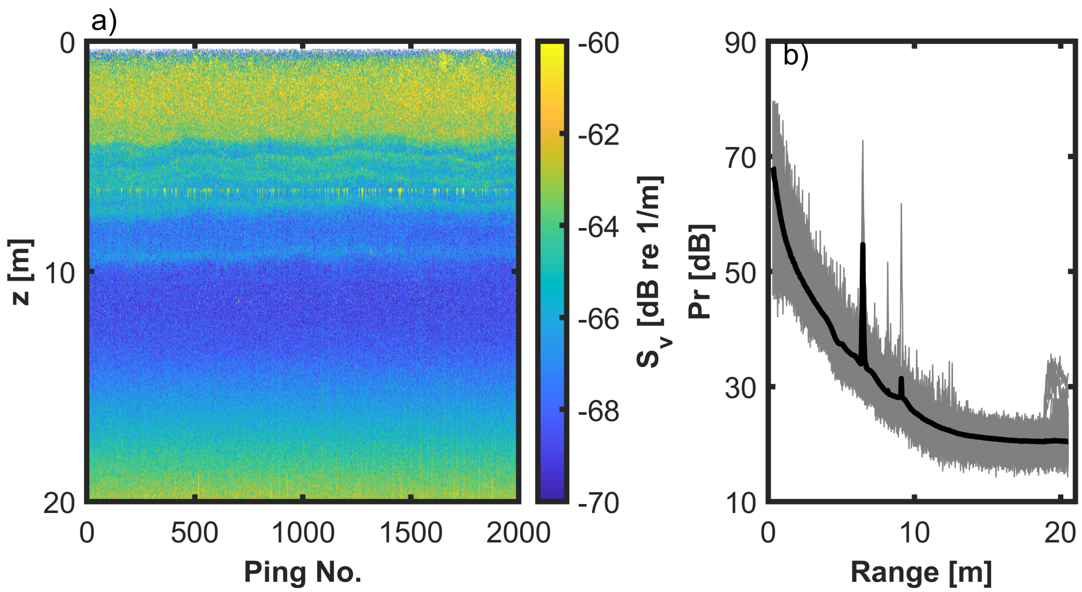

Figure 12: (a) Echogram of S_v from a calibration measurement. Below 15 m there is an increase in the apparent backscattering intensity that is constant across all pings, indicating that the results driven by the various scalar terms for range and volume correction are being applied to the noise floor. (b) P_r values for all pings shown in (a). With the exception of a few noise spikes, beyond approximately 15 m the signals are flat, indicating the noise floor has been reached. Note that if the volume backscattering was constant across this range, P_r would decrease by more than 5 dB between 15 and 20 m due to a combination of spreading and attenuation.

The ideal way to measure the system's noise floor is for the system to passively record the environment (i.e., perform measurements similar to those during active pinging, but during a period where no ping has been transmitted). In the absence of passive measurements, the noise must be estimated by identifying periods in the measurements where the noise floor has been reached. Two examples indicating that the noise floor has been reached are shown in Figure 12a. The first shows an echogram of S_v from one of the calibration measurements. In the upper water column, to a depth of approximately 10 m, one can see scattering from the sphere and other water column structure. Below approximately 15 m there is a gradual increase in apparent scattering with depth. This horizontal banding is a result of the time varying gain terms being added to the noise floor, which is otherwise assumed to be constant. Here we assume this represents the system's noise floor.

Similarly, a review of the received power levels can provide an indication of the noise floor. Once the system's noise floor has been reached the received power will be flat, with some noise, as a function of range. Figure 12b shows the P_r values as a function of range for every ping in Figure 12a. Beyond 15 m the measured P_r values are flat, with the exception of a few noise spikes visible in Figure 12a. Excluding these noise spikes the total range of P_r values is within approximately 3 dB of the mean. Figures 12a and b both indicate that the noise threshold in this context limits the useful range of the system to less than 15 m without accounting for SNR. This explains the horizontal banding structure seen in Figure 12a.

Having identified a range and set of pings beyond which the measurements indicate the noise floor, a NT value is calculated. This is done by taking a simple arithmetic average over a set of

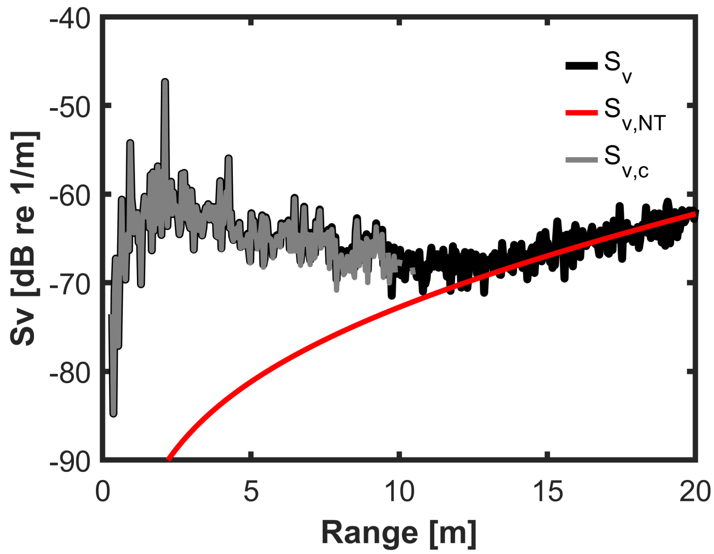

Figure 13: A comparison between the measured S_v, $S_{v,NT}$, and the final $S_{v,c}$, which includes the noise correction and the removal of data with SNRs less than 3 dB.

ranges and pings that only include measurements assumed to be the noise floor. In this case we have chosen to average values for the 500 pings at ranges greater than 18.2 m. The ping limit is set to avoid numerous noise spikes appearing at this depth range for pings later in the data set. The range limit of 18.2 m was chosen simply because it is further from the echosounder so the impacts of spreading and attenuation make it more likely to be operating in the noise floor. From these 25551 values we estimate $NT = 20.3$ dB. This calculation was performed for all six SWIFTs, using the same number of data points at the same ranges, and the NT values were 19.3 , 18.5 , 19.4, 20.3, 18.5, and 19.4 dB for SWIFT buoy numbers 21-26 and 28, respectively. The mean value of the six measurements is 19.3 dB.

Using this value, a new term, $S_{v,NT}$, is calculated by inserting NT into Equation 3. By replicating the general processing for S_v using the noise threshold it allows for direct comparison to scattering measurements, and subtraction of $S_{v,NT}$ from S_v to calculate a corrected term, $S_{v,c}$, where the subscript $_c$ denotes the corrected value with the noise subtracted. A comparison between the measured S_v and $S_{v,NT}$ (Fig. 13) shows that at ranges beyond 15 m the noise threshold and measured S_v are of the same magnitude. Furthermore, at ranges greater than 10 m the SNRs are less than 3 dB. Note that this doesn't generally indicate the system cannot operate to ranges greater than 10 m. Rather, doing so would require a combination of stronger scatterers, increased power level, or lower noise (which may not be possible).

Once $S_{v,NT}$ is calculated, the noise can be removed from S_v. This noise corrected curve is calculated according to

$$S_{v,c} = 10 \log 10 \left(10^{S_v/10} - 10^{S_{v,NT}/10} \right). \tag{13}$$

Note that the $10^{S_v/10} - 10^{S_{v,NT}/10}$ term can, in general, be negative due to noise fluctuations. Prior to calculating the logarithm these negative terms can be replaced with small, but non-zero, positive numbers (e.g., 10^{-16}) that are well below those that the system can resolve. As a final step we take the $S_{v,c}$ array and perform basic thresholding to suppress low SNR data. Here, we choose

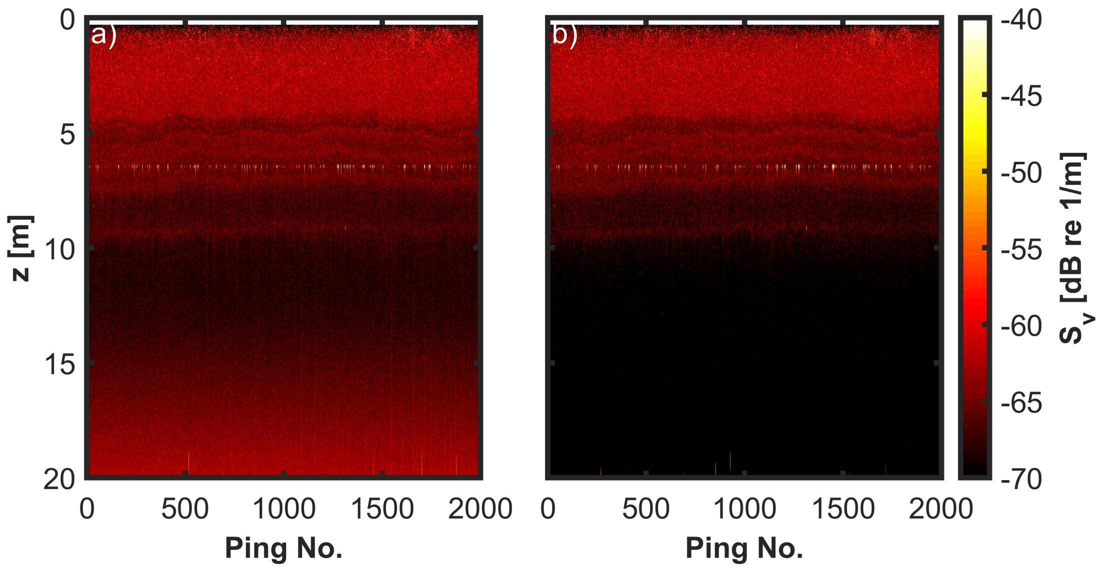

Figure 14: (a) Echogram of S_v with no correction for the noise threshold of the echosounder. (b) An echogram showing $S_{v,c}$ with the same data as (a) after the subtraction of the noise and thresholding for SNRs of 3 dB. Note that below approximately 10 m most of the data has been removed due to the SNR threshold, but occasional noise spikes are still clear in the data. Notably, this approach removes the horizontal bands associated with application of the time varying gain terms to the data near the noise threshold of the system.

an arbitrary threshold of 3 dB and replace all data points where $S_v - 3(\mathrm{SNR}) - S_{v,NT} < 0$ with a value of –150 dB re 1/m, which is well below levels that can be resolved by the system. Figure 13 includes an example of this corrected and thresholded $S_{v,c}$ value to the initial S_v and $S_{v,NT}$ curves while Figure 14 shows echograms before and after noise correction and thresholding. At short ranges and where the scattering is elevated, the subtraction of the noise threshold has little impact on the curve, but this correction becomes increasingly important near the noise limit of this system. This is particularly true if choosing not to apply a SNR threshold to the data.

As previously mentioned, the approach taken here to correct for the noise threshold is nearly identical to the method discussed in De Robertis and Higgenbottom [36], but alternative approaches have been adopted. [37;38] The literature contains additional details and valuable discussion regarding approaches to noise identification and removal.

The codes provided for post-processing of S_v measurements include noise correction and removal using the mean noise threshold of the six SWIFTs that were calibrated. This value, 19.3 dB, differs from the measured values by 1 dB or less for all units. A threshold SNR of 3 dB is also applied as was the case with the examples provided here. The implementation of the codes is relatively simple and these terms would be easy to modify for other experiments or instruments using the current codes.

7 RECOMMENDATIONS FOR FUTURE WORK

The Nortek Signature series ADCPs with echosounding capabilities are being adopted by an increasing number of users, but quantitative results derived from the units, of any frequency, are limited. In fact, we are aware of only one study presenting results from a calibrated Signature series echosounder.[21] Much remains to be learned about the system and a concerted effort to perform engineering measurements on the system to better understand its performance is recommended. Similar studies addressing the performance of newly developed echosounders and differences in the operating modes have been performed in the past[17;39] and yielded valuable information to inform their use. Such analysis would yield limited gains for qualitative use, but would make meaningful contributions to those interested in using the systems for quantitative purposes. An effort to broadly characterize the Nortek Signature series echosounder could include some of the following components:

- Measurements of transmit signal amplitudes to verify linearity between power levels
- Measurements of transmit signals across different durations to identify frequency content and stability in amplitude (i.e., compare the theoretical transmit signals to measured signals)
- Mapping of the beams to compare the theoretical values to those associated with the units
- Measurements to verify linearity of received signals
- The use of the noise thresholds (NT) for noise subtraction should be re-evaluated based on additional deployments to ensure the values are sufficiently representative of measurements in other environments
- Comparison between units to understand biases if a generalized gain value were to be applied to an otherwise uncalibrated unit

Such measurements performed across individual units and models would be helpful in determining uncertainties when working with multiple units.

In our experiments with Signature1000 echosounders on SWIFTs we chose not to implement motion correction. This decision was driven by the high degree of motion of the SWIFTs. In practice, this motion smears the apparent depth of scatterers vertically in the water column, but due to the total operational range of the instrument the net impact in the apparent depth is typically small, as shown by the ping-to-ping variability in scattering (Section 8). On a more stable platform, where the echosounders are ensonifying roughly the same portion of the water column, accounting for the platform's orientation is recommended.

8 APPLICATION AND EXAMPLES

Based on the system operations and equations in the preceding sections, several Matlab functions were developed (Appendix A) to convert the echosounder outputs to point and volume scattering measurements. This section provides a few examples of S_v echograms calculated from a deployment of the SWIFT drifters in Mobile Bay during the UnderSea Remote Sensing (USRS) DRI. In these examples, the standard S_v and time outputs from the files (.mat) were loaded and combined with other data to provide additional context for the echosounder measurements. The additional data used for this context include ADCP profiles from the Signature1000s and CTD profiles taken using Sontek Castaway units hand-deployed from the vessel managing the SWIFT deployments and recoveries. These observations are also supported by unpublished data using Simrad EK80 echosounders, microstructure profilers, CTD arrays, and an ADCP on another vessel involved in the experiment; they are qualitatively similar to the measurements and interpretation of estuarine scattering mechanisms discussed in Bassett et al. (2003).[8]

The measurements are shown in Figures 15–18, which include commentary in their captions. This commentary focuses on probable sources for the observed backscattering in the echograms. If present, a black dashed line in each of the echograms denotes the time at which a CTD was taken. If not shown the closest profile did not occur within the window of the SWIFT data.

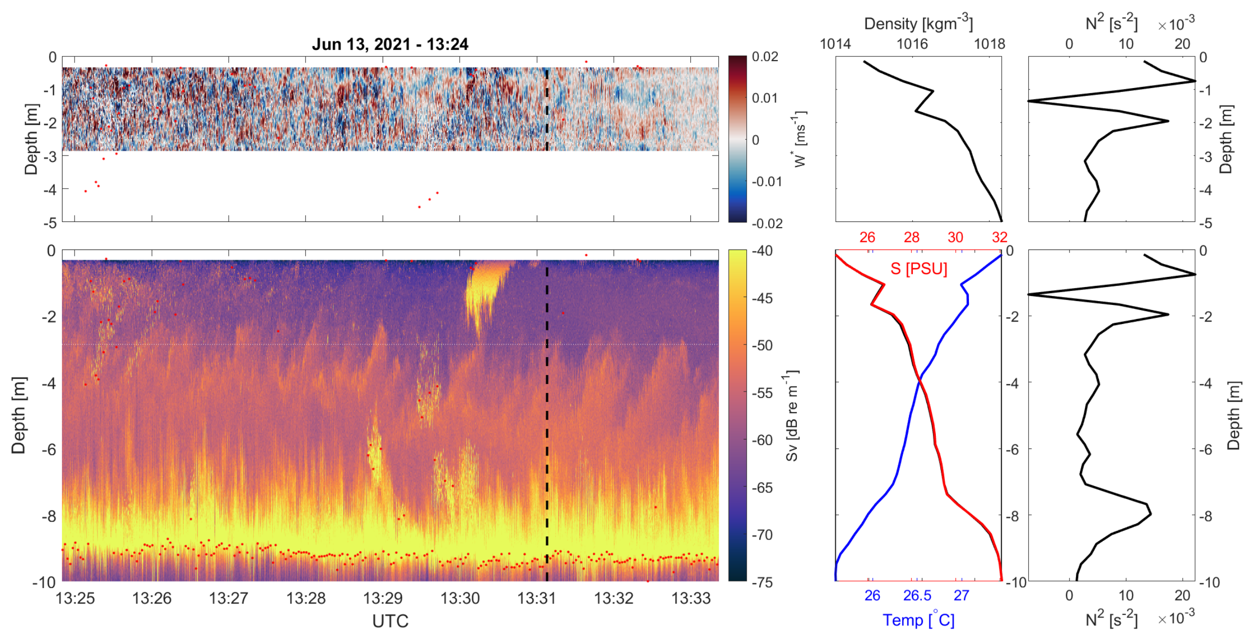

Figure 15: Example echogram showing numerous features including stratification of the water column, elevated suspended sediment near the seabed, and a bubble plume near the surface between 13:30 and 13:31. Smaller patches of elevated scattering in the water column away from the seabed are attributed to biological scatterers.

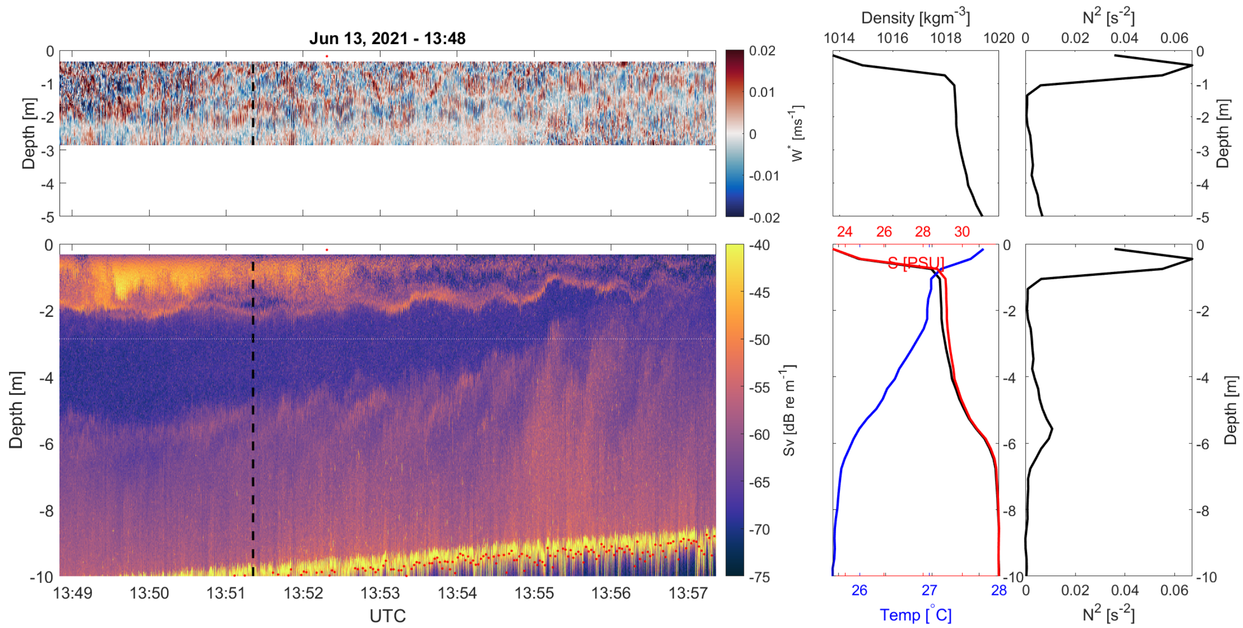

Figure 16: Echogram showing a water column composed of three different water masses. The upper mass contains high levels of scattering attributed to a mix of bubbles and microstructure. The intermediate layer shows weak scattering due to the weak temperature and salinity gradients. The bottom water mass also has weak gradients but does have elevated levels of scattering compared to the intermediate layer, which is attributed to elevated concentrations of suspended particulate. The layers are all easily distinguished acoustically.

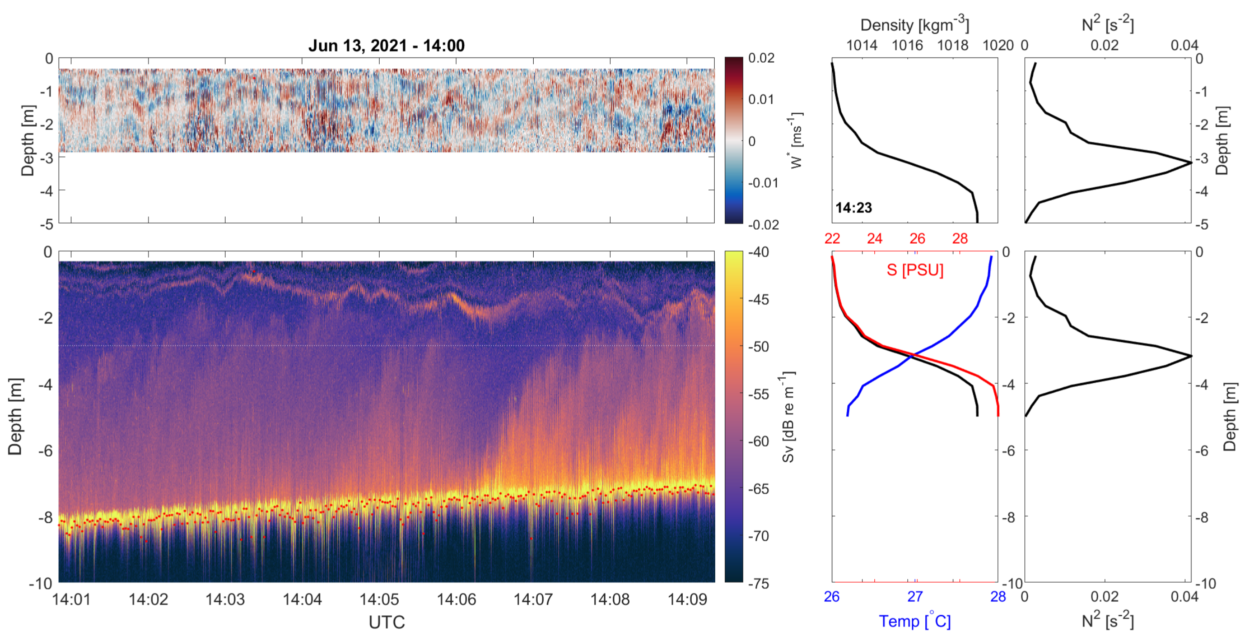

Figure 17: An example echogram showing numerous clines under-sampled by the CTD in the upper water column and elevated suspended particulate throughout much of the water column.

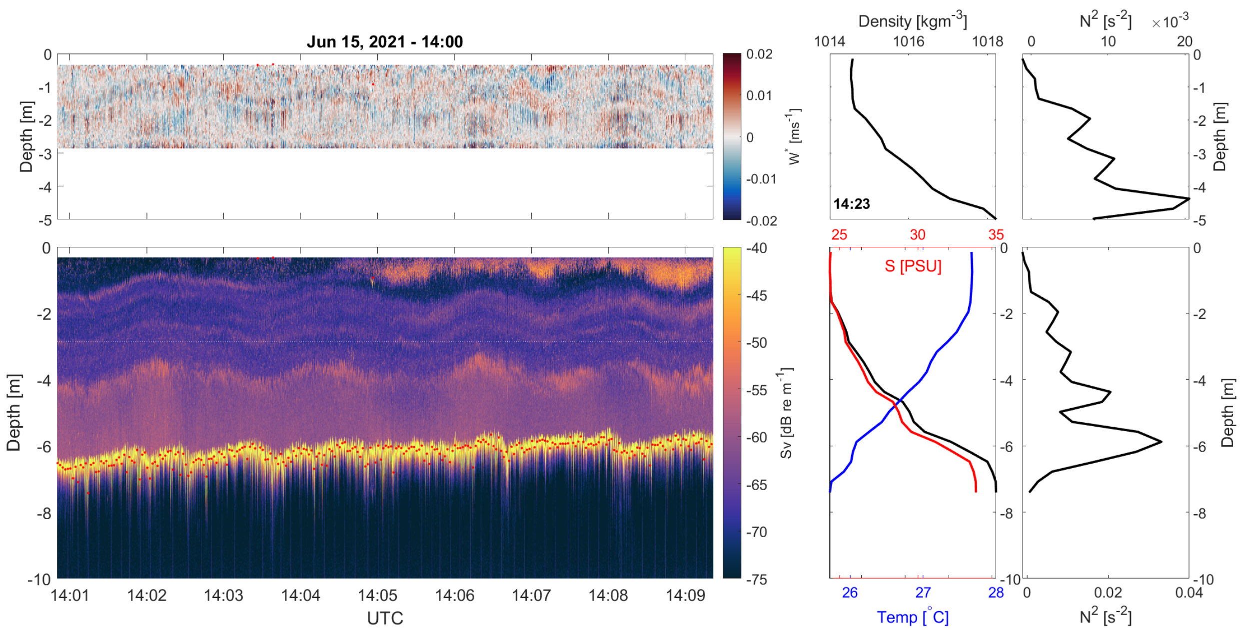

Figure 18: An echogram revealing numerous interfaces in the stratified water column. The source of the elevated backscattering in the upper water column is unknown.

REFERENCES

[1] J. Thomson. Wave breaking dissipation observed with "SWIFT" drifters. *J. Ocean. Atmos. Tech.*, 29(12):866–1882, 2012. doi: 10.1175/JTECH-D-12-00018.1.

[2] J. Thomson, M. Moulton, A. de Klerk, J. Talbert, M. Guerra, S. Kastner, M. Smith, M. Schwendeman, S. Zippel, and S. Nylund. A new version of the swift platform for waves, currents, and turbulence in the ocean surface layer. In *2019 IEEE/OES Twelfth Current, Waves and Turbulence Measurement (CWTM)*, pages 1–7, 2019. doi: 10.1109/CWTM43797.2019.8955299.

[3] T.K. Stanton, P.H. Wiebe, D. Chu, and L. Goodman. Acoustic characterization and discrimination of marine zooplankton and turbulence. *ICES J. Mar. Sci.*, 51:469, 1994.

[4] A.C. Lavery, P.H. Wiebe, T.K. Stanton, M.C. Bewnfield, and N. Copley. Determining dominant scatterers of sound in mixed zooplankton populations. *J. Acoust. Soc. Am.*, 122:3304—-3326, 2007. doi: 10.1121/1.2793613.

[5] A.C. Lavery, D. Chu, and J. Moum. Measurements of acoustic scattering from zooplankton and oceanic microstructure using a broadband echosounder. *ICES J. Mar. Sci.*, 67:379–394, 2010. doi: 10.1093/icesjms/fsp242.

[6] A. De Robertis, D.R. McKelvey, and P.H. Ressler. Development and application of an empirical multifrequency method for backscatter classification. *Can. J. Aqua. Fish. Sci.*, 67:1459–1474, 2010. doi: 10.1139/F10-075.

[7] T.K. Stanton. 30 years of advances in active bioacoustics: A personal perspective. *Methods Ocean.*, 1–2:49–77, 2012. doi: 10.1016/j.mio.2012.07.002.

[8] C. Bassett, A.C. Lavery, D. Ralston, W.R. Geyer, J.T. Jurisa, J. Thomson, D.A. Honegger, A. Simpson, M.E. Scully, and M.C. Haller. Acoustic backscattering at a tidal intrusion front. *Prog. Ocean.*, page 103167, 2023. ISSN 0079-6611. doi: 10.1016/j.pocean.2023.103167.

[9] E.J. Simmonds and D.N. MacLennan. *Fisheries Acoustics*. Blackwell Science, Oxford, UK, 2nd edition, 2005.

[10] L.R. Dragonette, S.K. Numrich, and L.J. Frank. Calibration technique for acoustic scattering measurements. *The Journal of the Acoustical Society of America*, 69(4):1186–1189, 1981. doi: 10.1121/1.385699.

[11] K.G. Foote. Optimizing copper spheres for precision calibration of hydroacoustic equipment. *The Journal of the Acoustical Society of America*, 71(3):742–747, 1982. doi: 10.1121/1.387497.

[12] D.A. Demer, L. Berger, M. Bernasconi, E. Bethke, K. Boswell, D. Chu, and Domokos, R. et al. Calibration of acoustic instruments. *ICES CRR No. 326*, 2015. doi: 10.25607/OBP-185.

[13] A.C. Lavery, C. Bassett, G. Lawson, and J.M. Jech. Exploiting signal processing approaches from broadband echosounder. *ICES J. Mar. Sci.*, 75(8):2262–2275, 2017. doi: 10.1093/icesjms/fsx155.

[14] V.C. Anderson. Sound scattering from a fluid sphere. *J. Acous. Soc. Am.*, 22(4):426–431, 1950. doi: 10.1121/1.1906621.

[15] J.J. Faran. Sound scattering by solid cylinders and spheres. *J. Acoust. Soc. Am.*, 23:405–418, 1951.

[16] T.K. Stanton and D. Chu. Calibration of broadband active acoustic systems using a single standard spherical target. *The Journal of the Acoustical Society of America*, 124(1):128–136, 2008. doi: 10.1121/1.2917387.

[17] D.A. Demer, L.N. Andersen, C. Bassett, L. Berger, D. Chu, and J. Condiotty et al. 2016 USA–Norway EK80 workshop report: Evaluation of a wideband echosounder for fisheries and marine ecosystem science. *ICES Coop. Res. Rep. No. 336*, 2017. doi: 10.17895/ices.pub.2318.

[18] D.N. MacLennan, P.G. Fernandes, and . Dalen. A consistent approach to definitions and symbols in fisheries acoustics. *ICES Journal of Marine Science*, 59(2):365–369, 3 2002. doi: 10.1006/jmsc.2001.1158.

[19] D. Chu and T. Stanton. Application of pulse compression techniques to broadband acoustic scattering by live individual zooplankton. *J. Acoust. Soc. Am.*, 104:39–55, 1998.

[20] L.N. Andersen, C. Dezhang, H. Heimvoll, R. Korneliussen, G.J. Macaulay, and E. Ona. Quantitative processing of broadband data as implemented in a scientific splitbeam echosounder. *arXiv*, 2021. doi: 10.48550/arXiv.2104.07248.

[21] G.R. Cutter, C.S. Reiss, S. Nylund, and G.M. Watters. Antarctic krill biomass and flux measured using wideband echosounders and acoustic doppler current profilers on submerged moorings. *Frontiers in Marine Science*, 9:1–23, 2022. doi: 10.3389/fmars.2022.784469.

[22] Nortek. Principles of Operation - Signature. 2022-08-15, pp. 34.

[23] H. Medwin and C. Clay. *Fundamentals of Acoustics Oceanography.* Academic Press, Boston, MA, 1998.

[24] K.G. Foote. Linearity of fisheries acoustics, with addition theorems. *J. Acoust. Soc. Am.*, 73 (6):1932–1940, 1983. doi: 10.1121/1.389583.

[25] J.E. Ehrenberg and T.C. Torkelson. Fm slide (chirp) signals: a technique for significantly improving the signal-to-noise performance in hydroacoustic assessment systems. *Fisheries Research*, 47:193–199, 2000.

[26] K.G. Foote, H.P. Knudsen, G. Vestnes, D.N. MacLennan, and E.J. Simmonds. Calibration of acoustic instruments for fish density estimation: a practical guide. 1987. doi: 10.17895/ices.pub.8265. URL https://ices-library.figshare.com/articles/report/Calibration_of_acoustic_instruments_for_fish_density_estimation_a_practical_guide/18624767.

[27] N.P. Fofonoff and R.C. Millard. Algorithms for computation of fundamental properties of seawater. Technical Report 44, Unesco Technical Papers in Marine Science, 1983.

[28] G. Turin. An introduction to matched filters. *IRE Trans. Inf. Theory*, 6(3):311–329, 1960. doi: 10.1109/TIT.1960.1057571.

[29] R.E. Francois and G.R. Garrison. Sound absorption based on ocean measurements: Part i: Pure water and magnesium sulfate contributions. *J. Acoust. Soc. Am.*, 72:896–907, 1982.

[30] R.E. Francois and G.R. Garrison. Sound absorption based on ocean measurements. part ii: Boric acid contribution and equation for total absorption. *J. Acoust. Soc. Am.*, 72:1879–1890, 1982.

[31] S. Vagle, K.G. Foote, M.V. Trevorrow, and D.M. Farmer. A technique for calibration of monostatic echosounder systems. *IEEE Journal of Oceanic Engineering*, 21(3):298–305, 1996. doi: 10.1109/48.508160.

[32] J.M. Jech, K.G. Foote, D. Chu, and L.C. Hufnagle. Comparing two 38-kHz scientific echosounders. *ICES Journal of Marine Science*, 62(6):1168–1179, 01 2005. doi: 10.1016/j.icesjms.2005.02.014.

[33] T.K. Stanton, D. Chu, J.M. Jech, and J.D. Irish. New broadband methods for resonance classification and high-resolution imagery of fish with swimbladders using a modified commercial broadband echosounder. *ICES J. Mar. Sci.*, 67:365–378, 2010.

[34] J.S. Renfree, L.N. Andersen, G. Macaulay, T.S. Sessions, and D.A. Demer. Effects of sphere suspension on echosounder calibrations. *ICES Journal of Marine Science*, 77(7-8):2945–2953, 2020. doi: 10.1093/icesjms/fsaa171.

[35] C. Bassett, A.C. Lavery, T.K. Stanton, and E.D. Cotter. Frequency- and depth-dependent target strength measurements of individual mesopelagic scatterers. *The Journal of the Acoustical Society of America*, 148(2):EL153–EL158, 8 2020. doi: 10.1121/10.0001745.

[36] A. De Robertis and I. Higginbottom. A post-processing technique to estimate the signal-to-noise ratio and remove echosounder background noise. *ICES J. Mar. Sci.*, 64(6):1282–1291, 2007. doi: icesjms/fsm112.

[37] J.L. Watkins and A.S. Brierley. A post-processing technique to remove background noise from echo integration data. *ICES J. Mar. Sci.*, 53(2):339–344, 1996. doi: 10.1006/jmsc.1996.0046.

[38] Rolf J. Korneliussen. Measurement and removal of echo integration noise. *ICES J. Mar. Sci.*, 57(4):1204–1217, 2000. doi: 10.1006/jmsc.2000.0806.

[39] A. De Robertis, C. Bassett, L.N. Andersen, I. Wangen, S. Furnish, and M. Levine. Amplifier linearity accounts for discrepancies in echo-integration measurements from two widely used echosounders. *ICES J. Mar. Sci.*, 76(6):1882–1892, 2019. doi: 10.1093/icesjms/fsz040.

[40] P. Morgan. SEAWATER: A library of MATLAB computational routines for the properties of sea water, 1994.

A CODE LIBRARY

The codes developed to perform the calibrations and the bulk processing of files to produce S_v and TS echograms have been uploaded to GitHub (https://github.com/SASlabgroup/SWIFT-codes/tree/master/Signature/Echo). All of the scripts are functions written in MATLAB. The archive includes a text file summarizing all scripts in the library. Descriptions of the files are also included here. Each script is well-commented and relates the implementation to specific equations and references included in this document. Over time these scripts may be developed further, particularly if modifications to firmware occur. Likewise, functionality may be added to accommodate different data formats (e.g., raw signals). Regardless, the use of the SONAR equation is well established for these applications so significant modifications to the implementation are unlikely.

Two main codes are used to produce S_v and TS echograms (Equations 3 and 1b, respectively, Section 2). These codes have numerous dependencies on other functions but are intended to be integrated directly into the overall SWIFT processing scripts, or in additional post-processing steps using archived outputs from those scripts. This section begins by summarizing the inputs to the S_v processing script then summarizing the TS processing script. All additional supporting functions are then presented.

Volume Scattering (S_v): The function to calculate the volume scattering is called *sigecho_vol*, which has inputs from processed echosounder arrays, physical measurements associated with the SWIFT, water properties, flags for processing options, and input and output directories. Many of these are optional and the scripts will revert to default properties if nothing is provided. The variable inputs include:

- *echo*: *echo* is a structure. While it contains many additional variables from the SWIFT processing, the key values and their dimensions are *echo.time* [$1xn$] – a time vector for the pings; *echo.CellSize* [$1x1$] – the range bin size; *echo.Blanking* [$1x1$] – the programmed blanking distance; and *echo.Echosounder* [nxm] – the P_r values, where n is the number of pings and m the number of range bins.
- *avg*: *avg* is a variable containing the Signature1000 average data type. It contains many variables irrelevant to the echosounder processing. In fact, the only value extracted from *avg* is *avg.AltimeterDistance*, which includes the distance to the seabed from burst data. Note that this altimeter data is not actually an average as the variable name suggests. It is measured for each ping. Its dimensions are [$1xn_a$], where n_a is smaller than the total number of pings. This variable is only used when a processing flag is called that identifies the range to the seabed and removes (writes NaN) values greater than 1 m below the inferred seabed.
- *z_off*: A [$1x1$] variable that is the depth of the transducer below the surface. This value is simply used to map the range bins onto depths relative to the free surface. A value of 0.2 m is assumed if no input is provided.
- w: A structure w containing water properties include salinity ($w.S$ in ppt), temperature ($w.T$ in °C), pH ($w.pH$), and depth ($w.z$ in m). Note that the latter should be specified as the mean depth over which the unit samples. These properties are used to calculate sound speed and attenuation. Single values representative of the water column are used. If no values are provided the system chooses default values of S = 30 ppt, T = 10°C, pH = 8.1, and z = 10 m.

- *ops*: A structure containing four flags for processing options: *ops.gainflag*, *ops.printflag*, *ops.exportflag*, and *ops.bot*. When *ops.gainflag* = 1 the processing code will use the gain value associated with the SWIFT buoy number, otherwise it will use the average of all available gain values. When *ops.printflag* = 1 echograms for the echosounder data are printed and saved. For *ops.exportflag* = 1 a new data file containing only variables for the pings, depth, and S_v used in the echogram will be exported. When *ops.bot* = 1 data will be processed to remove scattering values greater than 1 m below the seabed. If used in deep water, set *ops.bot* = 0. Note when *ops.bot* = 1, the exported data do not include NaN values below the seabed. If future work shows that identified noise thresholds are not suitable, an additional option for noise corrections could be integrated along with specific calls for modifying NT.
- *fn*: The name of the raw file being processed. This filename is used to identify the SWIFT buoy number and to output echograms and .mat files with the S_v data that follow the naming convention. The *fn* variable should include the directory structure for export.
- *outdir*: If the desired directory for the output varies from that of the data file an alternative directory can be provided. If no desired output directory is provided the scripts write any outputs to the same directory as the file being processed.

With these variables, the script will implement the volume backscattering equations, offset by the calibration gains, and produce all flagged data streams. To do so the code will call functions including *sw_svel*, *alpha_sea*, and if flagged *sig_makebot*, which will calculate the sound speed, attenuation, and perform the sub-bottom data removal, respectively.

Target Strength (TS): The target strength echogram code, *sigecho_target* is similar to the *sigecho_vol* code and requires all of the same inputs. The main difference between the processing scripts is that it implements Equation 1b instead of Equation 3, which is used to calculate the S_v echogram. In addition, the script calls a different set of gain values. At present, this script is not recommended because processing of the calibration data does not include a rigorously calculated on-axis gain value. It is possible to use this code with added uncertainty. Nonetheless, this processing option has been included to facilitate TS echograms if future system parameters and calibrations are better suited for the application. Note that calculations of TS using the Signature1000 units will inherently suffer from bias associated with off-axis targets and the lack of array processing potential to account for their position within the beam.

sig_makebot: The *sigecho_makebot* script is added to provide additional functionality to the S_v and TS processing scripts. It creates no new data and takes the S_v values calculated from *sigecho_vol*, in addition to the *echo* and *avg* structures, the depth vector z (calculated in both *sigecho_vol* and *sigecho_target*), and the *z_off* values. The script uses the ADCP's altimeter as a first estimate of the range to the seafloor, then removes outliers greater than three standard deviations from the mean, and interpolates the burst-averaged altimeter depth onto the full time series associated with the S_v or TS data. Once the interpolated range to the bottom is established, the transducer depth is accounted for and a 1-m offset below the seabed is added. All values of S_v or TS greater than 1 m below the seabed are replaced with NaN values.

sw_svel: This script calculates the sound speed of water following Fofonoff and Millard[27] and is written to provide seawater property routines prepared by CSIRO.[40] The water properties provided in the w structure are passed to this function to calculate the local sound speed to recalculate the range bins.

alpha_sea: *alpha_sea* takes the water properties and calculates the attenuation using the Francois and Garrison formulations.[29;30]